Schistosoma mansoni infection reprograms the metabolic potential of the myeloid lineage in a mouse model of metabolic syndrome

Diana Cortes-Selva[1], Lisa Gibbs[1], J. Alan Maschek [5,6], Tyler Van Ry[3,5], Bartek Rajwa[2], James E. Cox[3,5], Eyal Amiel[4], Keke C. Fairfax [1,7]

[1] Department of Pathology, Division of Microbiology and Immunology, University of Utah, Salt Lake City UT, 84112
[2] Bindley Bioscience Center, Purdue University, West Lafayette IN, 47907
[3] Department of Biochemistry, University of Utah, Salt Lake City UT, 84112
[4] Department of Biomedical and Health Sciences, University of Vermont, Burlington, VT 05405
[5]Metabolomics, Proteomics and Mass Spectrometry Cores, University of Utah, Salt Lake City, UT, 84112
[6] Department of Nutrition and Integrative Physiology and the Diabetes and Metabolism Research Center, University of Utah, Salt Lake City, UT 84112

Running title: Schistosomes reprogram myeloid metabolism

[7]Lead contact:

Keke Fairfax
Department of Pathology
Division of Microbiology and Immunology
University of Utah
JMRB 2200B
15 N Medical Drive East
Salt Lake City, UT 84112
Email: keke.fairfax@path.utah.edu
ORCID: https://orcid.org/0000-0002-8382-2960
801-581-5980 (office)

Keywords: Myeloid lineage, macrophage metabolism, *Schistosoma mansoni*, biological sex, metabolic disease

Summary

Despite evidence that helminths protect from metabolic disease, a major gap exists in understanding the underlying mechanism(s). Here we demonstrate that bone marrow derived macrophages (BMDM) from *S. mansoni* infected male ApoE$^{-/-}$ mice have dramatically increased mitochondrial respiration compared to those from uninfected mice. This change associates with increased glucose and palmitate shuttling into TCA cycle intermediates and decreased accumulation of cellular cholesterol esters. Moreover, systemic metabolic modulation by schistosomes is a function of biological sex, where infection protects ApoE$^{-/-}$ male, but not female, mice from obesity and glucose intolerance. Sex-dependence extends to myeloid cells, where reprogramming leads to opposite cholesterol phenotypes in BMDM from females and males. Finally, the metabolic reprogramming of male myeloid cells is transferrable via bone marrow transplantation to an uninfected host, indicating maintenance of reprogramming in the absence of sustained antigen exposure. This work reveals that *S. mansoni* systemic reprograming of myeloid metabolism is sex-dependent.

Introduction

Cardiovascular disease (CVD) is the leading worldwide cause of mortality (Hinton et al., 2018; Roth et al., 2017). In the United States, 65% of adults diagnosed with diabetes have elevated LDL cholesterol levels or take cholesterol lowering medications, and death rates from atherosclerotic cardiovascular disease (CVD) are ~1.7 times higher in this population as compared to non-diabetic adults (Emerging Risk Factors et al., 2010). It is well established that in the diabetic population, obesity, and dyslipidemia are risk factors underlying these increases in

68 mortality, while hyperglycemia is an independent risk factor (Marks and Raskin, 2000; Wong et
69 al., 2016). Underlying conditions such as diabetes and atherosclerosis contribute to the burden of
70 CVD in both females and males. While, the incidence of CVD is markedly higher in men than in
71 age-matched women (Opotowsky et al., 2007; Tan et al., 2010), the risk of developing CVD
72 while diabetic is much greater in women than men (Humphries et al., 2017; Peters et al., 2014).
73 In non-diabetic patients, females exhibit increased insulin sensitivity in comparison to males, as
74 well as reduced prevalence of dysglycemia and enhanced muscle glucose uptake (Cnop et al.,
75 2003; Kim and Reaven, 2013; Moran et al., 2008; Willeit et al., 1997), suggesting sex-dependent
76 modulations in whole body metabolism. Recent studies suggest a role of the gut microbiota in
77 the differences between sexes in the regulation of lipid metabolism (Baars et al., 2018).
78 Nevertheless, complete understanding of mechanistic basis behind sexual dimorphism in
79 metabolic syndrome is still lacking.
80
81 Previous studies have uncovered an association between a history of helminth infection and
82 reduced prevalence of metabolic disease in humans and rodents ((Doenhoff et al., 2002; Stanley
83 et al., 2009; Wiria et al., 2015). Specifically, infection by Schistosomes reduces cholesterol and
84 atherosclerotic plaques (Doenhoff et al., 2002; Stanley et al., 2009), this effect has been
85 attributed, in part, to an anti-inflammatory phenotype in macrophages (Wolfs et al., 2014) and
86 transcriptional reprogramming of phospholipid and glucose metabolism related genes in hepatic
87 macrophages (Cortes-Selva et al., 2018). Moreover, it has been postulated that schistosomes
88 have the potential to affect long term glucose metabolism in T cells (Chen et al., 2013).
89 Accumulating evidence suggests that biological sex affects disease progression; yet the effect of
90 schistosomiasis on metabolic-protection in females and males it is not well understood, as most

91 studies have been conducted only in males or no sex differentiation has been made during data
92 analysis ((Sanya et al., 2019; Shen et al., 2015; Wolde et al., 2019)). To date, no report with a
93 particular emphasis on females has been conducted.
94
95 Schistosomiasis induces Th2 polarization and alternative activation of macrophages, essential for
96 host survival (Barron and Wynn, 2011; Fairfax et al., 2012; Herbert et al., 2004). IL-4 induced
97 alternative activation of macrophages relies on oxidative phosphorylation (OXPHOS) and fatty
98 acid oxidation for energy production, and is dependent on cell intrinsic lysosomal lipolysis
99 (Huang et al., 2014; Vats et al., 2006). Macrophage metabolism follows a dysmorphic pattern, as
100 sex-related differences affect the processes involved in cholesterol and lipid metabolism in
101 macrophages as well as inflammatory cytokine production in adipose tissue (Griffin et al., 2016;
102 Ng et al., 2001). Moreover, in rats, phagocytes from females had increased ROS generation than
103 males (Rudyk et al., 2018). Such differences have often been attributed to the role of sex
104 hormones in gene expression and immune cell function (Rubinow, 2018; Taneja, 2018; Winn et
105 al., 2019), but a clear understanding of the effects of sex on the regulation of macrophage
106 metabolism, as well as how sex modulates the effects of schistosomiasis in the protection from
107 metabolic disease is lacking.
108
109 In the present study, we sought to determine the systemic effects of *S. mansoni* infection on the
110 myeloid lineage. Surprisingly, we discovered that macrophages derived from the bone marrow of
111 *S. mansoni* infected male mice have dramatically increased oxygen consumption and
112 mitochondrial mass compared to those from uninfected males. This shift is accompanied by
113 increased carbon shuttling into TCA cycle intermediates, a decrease in cholesterol esters, and

114 increased fatty acid oxidation. When we examined the role of biological sex in schistosome
115 induced modulation we found that *S. mansoni* infection does not reliably protect ApoE$^{-/-}$ female
116 mice from HFD induced weight gain or glucose intolerance. The sex-dependent effect of
117 infection extends to the myeloid lineage, where bone marrow derived macrophages from infected
118 females display the opposite metabolic phenotype as those from infected males, with a dramatic
119 increase in cellular cholesterol esters. Overall, these data present the first evidence that *S.*
120 *mansoni* systemically modulates the myeloid compartment in a sex-dependent manner and
121 provide a more comprehensive understanding of how *S. mansoni* infection may confer metabolic
122 protection at the cellular level.
123
124 **Results**
125 **Macrophages derived from *S. mansoni* infected male mice have increased oxygen**
126 **consumption and spare respiratory capacity**
127
128 We have previously reported that schistosomiasis alters the expression of numerous genes
129 relevant to glucose, cholesterol, and amino acid metabolism in hepatic macrophages of male
130 mice (Cortes-Selva et al., 2018). These alterations are associated with improved insulin
131 sensitivity and atherosclerotic score in male mice. Since it has previously been shown that
132 during *S. mansoni* infection the majority of liver macrophages are monocyte derived, and
133 monocyte recruitment drives both atherosclerosis (Potteaux et al., 2011; Tacke et al., 2007) and
134 obesity induced insulin resistance (Beliard et al., 2017; Liang et al., 2007; Oh et al., 2012; Rull et
135 al., 2010), we hypothesized that Schistosome infection may imprint the monocyte- macrophage
136 lineage with altered metabolic propensities. To elucidate whether infection imprints

137 macrophages with an altered metabolic phenotype we infected (and mock infected controls)
138 atherogenesis-prone male ApoE$^{-/-}$mice on high-fat diet (HFD), and sacrificed them at 10-weeks
139 post-infection to harvest bone marrow cells. Macrophages were differentiated *in vitro* with M-
140 CSF in a 6-7-day culture. We performed real-time extracellular flux analysis on unstimulated
141 bone marrow derived macrophages (BMDM) from ApoE$^{-/-}$ HFD infected and uninfected
142 (control) HFD mice to quantify oxygen consumption rate (OCR) (Figure 1A). BMDM from
143 ApoE$^{-/-}$ HFD infected mice showed improved basal respiration (Figure 1B) and significantly
144 increased spare respiratory capacity ($p<0.0001$, Figure 1C). Since eukaryotic cells integrate
145 oxidative phosphorylation (OXPHOS), glycolysis and the tricarboxylic acid (TCA) cycle to
146 satisfy energy requirements, we also tested the extracellular acidification rate (ECAR), which is
147 suggested as a marker of inhibited mitochondrial respiration (Pike Winer and Wu, 2014), in
148 BMDM from infected and uninfected ApoE$^{-/-}$ HFD mice. We observed no differences in ECAR
149 in infected male mice compared to uninfected controls (Figure 1D). Cell intrinsic lysosomal
150 lipolysis has previously been shown to support macrophage spare respiratory capacity in the
151 context of macrophage alternative activation (Huang et al., 2014; Liu et al., 2017). We stained
152 for hydrophobic and neutral lipids by Oil Red O (ORO) (Mehlem et al., 2013) and observed that
153 the lipid content of BMDM from infected ApoE$^{-/-}$ males trended to reduction in comparison to
154 the control group, but was not significantly reduced (Figure 1E). To analyze BMDM
155 mitochondrial mass, which has also been linked to increased respiratory capacity (Langston et
156 al., 2017), we analyzed mitochondrial activity by Mitotracker Deep Red FM. We observed that
157 BMDM from infected mice exhibited increased MitoTracker median fluorescent intensity (MFI)
158 in comparison to the BMDM from uninfected mice (Figure 1F). Overall, these data indicate that
159 *S. mansoni* infection in males leads to increased oxygen consumption and mitochondrial

160 metabolism in BMDM. Mitochondrial oxidative dysfunction in macrophages has recently been
161 linked to insulin resistance (Jung et al., 2018), so this metabolic shift could contribute to the
162 infection-induced improvement in glucose tolerance seen in infected males .
163
164 **Schistosomiasis in male ApoE$^{-/-}$ mice alters metabolic flux of glucose and the lipidomic**
165 **fingerprint of macrophages**
166
167 In order to understand how Schistosome infection alters the metabolic fingerprint and promotes
168 mitochondrial metabolism in macrophages derived from ApoE$^{-/-}$ HFD male mice, we performed
169 metabolic tracing analysis, where macrophages were differentiated in the presence of normal
170 glucose and then switched to ^{13}C-labeled glucose for 24 hours. We observed increased shuttling
171 of heavy labeled glucose to malate (Figure 2A), citrate (Figure 2B), itaconate (Figure 2C), and
172 succinate Figure 2E in BMDM from infected mice in comparison to BMDM from uninfected
173 mice. The lack of increased heavy lactate production (Figure 2D), suggests that the primary
174 reprogramming is focused on glucose-dependent mitochondrial metabolism. Importantly, we
175 found no upregulation of alternative activation markers (CD301, CD206, Arg1, Nos2) in
176 unstimulated BMDM from infected mice when compared to BMDM from controls
177 (Supplementary Figure 1). Since we have previously shown that infection alters the phospholipid
178 and cholesterol metabolism in hepatic macrophages (Cortes-Selva et al., 2018), we performed
179 unbiased lipidomics using liquid chromatography-mass spectrometry (LC-MS). We used a
180 supervised model by partial least squares-discriminant analysis (PLS-DA), with two components
181 to determine the lipidomic profile of BMDM. There was a robust separation between groups that
182 indicates the metabolic profiles of BMDM from infected and uninfected males differ

183 significantly and suggests that there is a prominent alteration of metabolites induced by infection
184 in male mice (Figure 2F). The lipid species that drive the variation observed in the PLS-DA as
185 measured by the Variable Importance in Projection (VIP) score from uninfected males in
186 comparison to infected males included cholesterol esters (CE) (20:1), CE (22:0), CE (24:0), CE
187 (24:1), CE (22:4), CE (22:1), CE (18:0); diacylglycerols (DG) (16:0_16:0), DG (16:0_18:0) and
188 triacyclglycerol (TG) (16:0_16:0_16:0) (Figure 2G,H). We then analyzed the total CE levels in
189 macrophages from both groups of male mice and found that infection led to significantly reduced
190 CE in male mice ($p<0.0001$, Figure 2I), further evidencing an important role of cholesterol
191 metabolism in macrophages following helminth infection. Next, we determined the
192 transcriptomic modifications induced by infection in unstimulated BMDM from infected and
193 uninfected males by mRNA sequencing (mRNAseq). Significant gene expression differences
194 were observed in BMDM from infected male mice, compared to uninfected controls. Transcripts
195 from the two groups are depicted in Volcano plots, using false discovery rate (FDR<0.05 in red,
196 FDR<0.01 in blue) and Log2 fold changes (cut off of .6 Log2 FC) to identify statistically
197 significant genes (Figure 2J). Among the differentially regulated factors are Gbp6, which is
198 related to interferon-γ signaling and innate immune function; Gm7609, a predicted pseudogene;
199 Gbp4, a member of the GTPase family involved in protective immunity against microbial and
200 viral pathogens; Apol9a, which is predicted to be related to lipid transport, lipoprotein metabolic
201 processes and stimulated by interferon; Iigp1, a GTPase with roles in response to intracellular
202 pathogens; CD300e, which belongs to families of paired activating and inhibitory receptors
203 implicated in immune responses; and Batf2, a basic leucine zipper factor whose activation is
204 detrimental for type-1 infectious disease. Importantly, Mgll, which encodes monoacylglycerol
205 lipase that catalyzes the conversion of monoacylglycerides to free fatty acids and glycerol was

206 significantly increased. Mgll is required for lipolysis and improved glucose homeostasis in mice
207 on HFD (Berdan et al., 2016; Douglass et al., 2015), an infection driven increase was validated
208 by RT-qPCR (Figure 2L). In addition, Slc1a3, which encodes for the glutamate aspartate
209 transporter 1 that is localized in the inner mitochondria membrane as part of the malate-aspartate
210 shuttle and is relevant for amino acid homeostasis in adipocytes, was significantly altered in our
211 model, and was further validated by RT-qPCR (Figure 2M). Interestingly, the pathways
212 significantly altered (Figure 2K) during infection included hematopoietic cell lineage ($p=5.779$
213 $x10^{-8}$), asthma ($p=3.169$ $x10^{-5}$), and cytokine-cytokine receptor interactions, graft-versus host
214 disease, type 1 diabetes and allograft regression ($p=0.0000894$). Together, these data identify key
215 factors in immune and metabolic responses as well as novel factors with unknown functions that
216 are regulated by exposure to *S. mansoni* infection.
217
218 ***S. mansoni* infection protects male mice, but not female mice, from obesity and glucose**
219 **intolerance independently of systemic alternative macrophage activation**
220
221 Sex is a key contributor to the phenotype of cardiovascular and metabolic features in mammals
222 (Chella Krishnan et al., 2018), so we assessed the sex dependent impact of *S. mansoni* infection
223 on obesity and glucose intolerance. For this, we fed male and female $ApoE^{-/-}$ HFD for 10-days
224 before infection. We infected and mock infected mice (controls) as described in the methods.
225 Ten weeks post infection we analyzed body weight and glucose tolerance (via an IP glucose
226 tolerance test) and found that infection is significantly beneficial for male, but not female mice,
227 as only males are protected from HFD-induced weight gain and glucose intolerance (Figure 3A,
228 3B). We also analyzed serum triglyceride (TG) and diglyceride (DG) levels using untargeted

229 lipidomics and found that relative abundance of both TG and DG were decreased in infected
230 males as compared to uninfected males, while TGs were increased by infection in females and
231 DGs were unchanged (Figure 3C). These data indicate that *S. mansoni* infection induces a sex-
232 dependent modulation of metabolic disease parameters. We then wondered if this infection-
233 mediated effect in males only was correlated with differences in systemic alternative activation
234 of hepatic macrophages in females. Flow cytometry analysis showed that alternative activation
235 markers (CD206, CD301, Arg1) were highly expressed in macrophages from male and female
236 mice following infection, but not in naïve mice (Figure 3D), suggesting that *S. mansoni* induced
237 alternative activation irrespective of sex. Previous studies characterizing the dynamics of
238 alternatively activated macrophages during schistosome infection have found that these
239 macrophages primarily arise from Ly6C^{high} monocytes (Girgis et al., 2014; Nascimento et al.,
240 2014). Naïve male and female ApoE$^{-/-}$ mice on HFD had equivalent frequencies of Ly6c^{high}
241 monocytes circulating in peripheral blood. At 10-weeks post infection we found an increased
242 percentage of both Ly6C^{int} and Ly6C^{high} cells (Figure 3E) in both male and female mice
243 compared to the mock infected controls, with the frequency of Ly6C^{high} cells in females 1.74
244 times that of males, suggesting either increased monopoiesis in females, or increased tissue
245 recruitment in males . Since we had found increased mitochondrial MFI in BMDM from infected
246 male mice, we asked whether circulating blood monocytes are similarly modulated. We observed
247 an infection induced increase in Mitotracker fluorescent intensity in monocytes from male ApoE^{-}
248 $^{/-}$ mice on HFD, but not from females (Figure 3F). These data suggest that there is sex-specific
249 increased mitochondrial activity following infection in the monocyte cell population. We then
250 wondered if these effects in the differentiated monocytes are the result of long-lasting changes in
251 the myeloid lineage after helminth infection. For this, we analyzed the main lineages of

252 hematopoietic progenitors that produce myeloid cells: granulocyte-monocyte progenitors (GMP),
253 monocyte-DC progenitors (MDP) and the common myeloid progenitor (CMP) in female and
254 male ApoE$^{-/-}$ mice. CMP were defined as Lin^{-}CD127^{-}c-Kit^{+}Sca-1^{-}CD34^{+}FcRII/III$^{lo/-}$(Paul et al.,
255 2016), GMP were defined as Lin^{-}IL-7R^{-}Sca-1^{-}c-kit^{+}CD34^{+}FcR II/III^{+}, and MDP were defined
256 as defined as Lin^{-} c-Kit^{+} Sca-1^{-} CD34^{+} FcγR^{lo} CD115^{hi} cells. Overall bone marrow cellularity
257 was not affected by Schistosome infection (Figure 3G), however, the numbers of CMP and GMP
258 in infected male mice were significantly reduced compared to uninfected controls, while GMP
259 and CMP were not reduced in females (Figure 3 H-J). The numbers and percentages of MDP
260 remained unchanged in infected females and males compared to uninfected controls (Figure 3K,
261 3L). These data suggest that *S. mansoni* infection modulates both metabolic disease and the
262 myeloid lineage in a sex-specific manner that is independent from the induction of systemic
263 alternative activation.
264
265 ***S. mansoni*-increases fatty acid oxidation in male but not female ApoE$^{-/-}$ mice on HFD**
266
267 In order to determine whether infection-induced pathologic differences in males and females
268 were accompanied by sex-specific differential macrophage metabolic regulation, we cultured
269 bone marrow cells from 10-week infected or uninfected control male and female mice for 7 days
270 to generate BMDM. OCR was measured in real time in basal conditions and following the
271 addition of mitochondrial inhibitors in unstimulated BMDM from both infected and uninfected
272 male and female ApoE$^{-/-}$ animals. Similar to as seen in Figure 1A, BMDM from infected males
273 exhibited increased basal OCR and spare respiratory capacity compared to uninfected male
274 controls (Figure 4A, 4B, 4C). However, basal OCR and spare respiratory capacity of BMDM

275 from infected females remained unaltered in comparison to BMDM from uninfected females
276 (Figure 4A, 4B, 4C). Moreover, side by side OCR analysis in females and males with palmitate
277 as a substrate (glucose limiting conditions) showed that BMDM from infected male, but not from
278 infected females had an increased ability to oxidize exogenous palmitate (Figure 4D). In
279 addition, BMDM from infected males but not females had significantly increased palmitate basal
280 OCR and palmitate spare respiratory capacity, suggesting exogenous free fatty usage as a carbon
281 source for OXPHOS (Figure 4E, 4F). Similar to the male only data, we observed no differences
282 in macrophage lipid content in either group, suggesting that global lipolysis may not underlie
283 OCR and spare respiratory capacity in our model (Figure 4G). Additionally, analysis of
284 mitochondrial mass in females and males showed that similar to blood monocytes, BMDM from
285 infected male mice, but not females have a significantly higher Mitotracker MFI. These data
286 suggest that *S. mansoni* infection improved mitochondrial biogenesis in males, but not females.
287 Again, suggesting differential regulation of macrophage metabolism based on biological sex.
288 This regulation may account in part for the differences in the role of infection in modulating
289 obesity and insulin sensitivity.
290
291 ***S. mansoni* infection differentially alters the cellular lipid profile in female and male mice**
292
293 To understand the sex specific modulations induced by schistosomiasis in macrophage lipid
294 metabolism, we isolated cellular lipids from unstimulated BMDM and performed unbiased
295 lipidomics in male and female derived-cells. PLS-DA showed that *S. mansoni* infection led to a
296 sex-specific lipid profile (Figure 5A). Further, analysis of total CE (identified as a VIP species in
297 males in Figure 2) showed that infection led to decreased levels of CE in cells derived from

298 infected male mice. In contrast, infection led to significantly increased total CE in BMDM
299 derived from infected female mice (Figure 5B). Similar to males, infection in females induces a
300 unique lipid signature (Figure 5C), with two species of plasmanyl-PE, three species of
301 plasmanyl-PC, BMP and CE as the main drivers of the altered lipid profile in females during
302 infection (Figure 5D). Since we observed BMP's as a VIP compound driven by *S. mansoni*
303 infection in females, but not males, we went back and performed targeted lipidomics to quantify
304 BMPs at the class level. Indeed, total BMPs were significantly increased by infection in BMDM
305 from females but not males (Figure 5E). Our Seahorse data indicates that *S. mansoni* infection
306 induced differential oxidation of exogenous palmitate in BMDM derived from males and
307 females. In order to understand the metabolic flux of exogenous palmitate, we performed
308 metabolic tracing analysis of palmitate, where macrophages were differentiated in the presence
309 of normal glucose and then switched to C^{13}-labeled palmitate for 24 hours. Similar to what we
310 documented with glucose, we observed increased shuttling of heavy labeled palmitate into
311 succinate, malate, and fumarate in BMDM derived from infected males, with decreased shuttling
312 into myristate (a marker of fatty acid elongation). BMDM derived from infected females
313 displayed the opposite phenotype, with decreased shuttling of heavy labeled palmitate into
314 succinate, malate, and fumarate, and increased shuttling into myristate compared to BMDM from
315 uninfected controls. These data suggest that BMDM derived from infected male $ApoE^{-/-}$ mice
316 have increased basal utilization of exogenous palmitate for beta-oxidation, while the female data
317 suggests increased lipid synthesis, strengthening the data obtained from our palmitate
318 extracellular flux analysis.
319 To further understand the role of biological sex in the *S. mansoni* induced reprograming of the
320 BMDM lipidome, we isolated cellular lipids from male and female BMDM either unstimulated

321 (media), or following LPS stimulation, and then performed untargeted lipidomics as described in
322 Figure 5. We analyzed the lipidomic data with machine learning using a two-step selection
323 process (see Methods). This approach identified ~20 features (lipid compounds) contributing to
324 an elastic net regression model that can predict the infection status of samples-originating
325 animals (Zou, 2005). These informative features are listed in descending order of importance
326 (Supplemental Figure 2A). Interestingly, some key features (for instance, the top scoring one) are
327 not represented as significant in the univariate tests (univariate adjusted p values, Supplemental
328 Figure 2B). However, these features are important contributors to the multivariate machine
329 learning model. This is not unexpected – some features that would be considered uninformative
330 individually may be very useful in improving predictions if combined with other features. When
331 we examine these features individually, we can see a differential response to infection for males
332 and females (for instance, PG 18:1_18:2, a glycerophospholipid) represented in Supplemental
333 Figure 2C). Seven of the 20 molecular features identified by machine learning are BMP
334 (Bis(monoacylglycerol)phosphate) species, which have been implicated in glycosphingolipid
335 degradation and cholesterol transport (Anheuser et al., 2019; Luquain-Costaz et al., 2013). These
336 data further support the hypothesis that *S. mansoni* infection differentially modulates the
337 metabolism of myeloid cells from male and female animals, and that this modulation revolves
338 around decreased cholesterol storage and fatty acid synthesis in males and increased cholesterol
339 storage and fatty acid synthesis in females. Cholesterol and lipid metabolism has previously been
340 associated with inflammatory myeloid effector function (Carroll et al., 2018; Funk et al., 1993;
341 Oiknine and Aviram, 1992), so we quantified the acute inflammatory effectors nitrite and iNOS,
342 along with pro-inflammatory cytokines/chemokines IL-12p70, CXCL1, and IL-6
343 (chemokines/cytokines with known pathogenic roles in obesity, insulin resistance and

344 atherosclerosis) following stimulation with LPS. *S. mansoni* infection increases LPS induced
345 nitrite and iNOS production in BMDM from male, but not female ApoE$^{-/-}$ mice on HFD (Figure
346 5 J,K). Conversely, BMDM from infected males have decreased production of IL-2p70, CXCL1,
347 and IL-6 (Figure 5 L-N) following LPS stimulation as compared to BMDM from uninfected
348 controls. LPS induced IL-12p70, CXCL1, and IL-6 production by female BMDM is unaffected
349 by infection status. Increased production of the effector molecules nitrite and iNOS combined
350 with decreased production of pro-inflammatory mediators associated with chronic inflammation
351 supports the idea that *S. mansoni* infection promotes a hybrid macrophage state in males.
352

353 ***S. mansoni* infection modulates the myeloid transcriptome in a sex-specific manner**

354 Since we documented significant sex dependent shifts in functional metabolism in BMDM from
355 male and female *S. mansoni* infected mice, we sought to determine if differential transcriptional
356 modulation underlies these shifts. In order to investigate the genes and respective pathways that
357 were associated with specific conditions and the ones that were differentially regulated by sex we
358 performed mRNAseq on unstimulated BMDM derived from male and female ApoE$^{-/-}$ mice at 10-
359 weeks post *S. mansoni* or mock infection. We identified different subsets of genes that were
360 preferentially upregulated in males ($p<0.05$, Figure 6A). Among 1448 genes upregulated in
361 males regardless of infection status with a p value <0.05, the majority of these (238 genes) were
362 associated to metabolic functions by pathway analysis. Of these 238 genes involved in
363 metabolism we identified hexokinase 1 (hk1), citrate synthase (cs), apolipoprotein A2 (apoa2),
364 aldehyde dehydrogenase 3 family member A2 (aldh3a2), lipoyltransferase (lipt1), solute carrier
365 family 19 member 1 (slc19a1), LDL receptor related protein 1 (lrp1), many of these are involved
366 in lipoprotein and cholesterol metabolism. These data suggest that myeloid metabolism is

367 differentially regulated by sex, at least in the context of HFD. In addition, we found 216 genes
368 involved in immunity. Among these genes with immune function we identified interleukin 10 (il-
369 10), Toll like receptor 5 (tlr5), NLR family pyrin domain containing 3 (nlrp3), inducible T cell
370 costimulatory (icos), which have diverse pro and anti-inflammatory function in the immune
371 system. Next, we surveyed the genes that are differentially regulated in males and females
372 following *S. mansoni* infection. We found 66 genes involved in metabolism, hemostasis, the
373 adaptive immune system, collagen degradation and not annotated to specific pathways.
374 Following the genes with known function, the majority (10) of differentially regulated genes
375 have documented roles in metabolism. Among these, we identified type II iodothyronine
376 deiodinase (dio2), which has been implicated in the regulation of diet induced obesity
377 (Kurylowicz et al., 2015; Vernia et al., 2013). Moreover, we found that hexokinase 3 (hk3), fatty
378 acid binding protein 4 (fabp4), sphingomyelin synthase 2 (sgms2), solute carrier family 6
379 member 8 (slc6a8) were all upregulated in male and downregulated in female BMDM following
380 *S. mansoni* infection (Figure 6B). In addition, we performed gene ontology analysis from the 66
381 genes that were differentially regulated in females and males. The most significant pathways
382 were response to glucocorticoids, glycoprotein metabolism, and fatty acid metabolism, again
383 suggesting that there is a sex-specific metabolic response to *S. mansoni* infection in myeloid
384 cells. These pathways may help explain the differential metabolic modulation induced by
385 schistosomiasis in males and females (Figure 6C).
386
387 ***S. mansoni* induced modulation of male macrophage metabolism is long-lived in the**
388 **absence of antigen**

389 Our metabolic and transcriptomic data from BMDM differentiated *in vitro* from male *S. mansoni*
390 infected mice suggested that metabolic modulation may be long-lived in the absence of ongoing
391 antigen exposure. In order to determine durable nature of modulation we transferred bone
392 marrow from either 10-week *S. mansoni* infected male ApoE$^{-/-}$ mice on HFD, or uninfected male
393 controls into busulfan treated recipient ApoE$^{-/-}$ mice on HFD. At 10 weeks post-bone marrow
394 transfer we assayed glucose tolerance via an i.p. GTT. Mice that received bone marrow from
395 infected males have a significantly lower glucose area under the curve (AUC) than those that
396 received control bone marrow. We harvested bone marrow from all recipients and differentiated
397 BMDM in M-CSF for 6 days and then performed real-time extracellular flux analysis. BMDM
398 from recipients of bone marrow from *S. mansoni* infected mice had significantly higher basal
399 oxygen consumption and a trend towards increased spare respiratory capacity as compared to
400 BMDM generated from recipients of uninfected control bone marrow. Additionally, BMDM
401 from recipients of bone marrow from *S. mansoni* infected mice had a significantly higher
402 Mitotracker MFI than BMDM from recipients of control bone marrow. These data suggest that *S.*
403 *mansoni* induced metabolic modulation of the myeloid lineage in males is long-lived even in the
404 absence of ongoing exposure to egg antigens, and that hematopoietic cells are at least partially
405 responsible for the regulation of whole-body glucose metabolism in the HFD ApoE$^{-/-}$ model.

406 **Discussion**

407 Helminth infections in general, and schistosomiasis in specific, have been known to be
408 inversely correlated with obesity and glucose intolerance for over a decade, a phenomenon
409 thought to be associated with Type 2 polarization of macrophages and T cells. In the current
410 study we report that *S. mansoni* infection induces dramatic metabolic alterations in BMDM from
411 male ApoE$^{-/-}$ mice on HFD. Our results indicate that macrophages derived from the bone marrow

412 of infected male mice have increased basal oxygen consumption and spare respiratory capacity
413 compared to those derived from uninfected males. In T cells, an increase in spare respiratory
414 capacity has been linked to mitochondrial biogenesis, and controls the transition to a long-lived
415 memory phenotype (van der Windt et al., 2012). In macrophages, M2 (alternative) activation has
416 previously been shown to lead to increased spare respiratory capacity, a process that also
417 involves mitochondrial biogenesis (Kannan et al., 2016), while TLR recognition of bacteria has
418 been shown to increase mitochondrial respiration via modulation of complex I and II (Garaude et
419 al., 2016) . In both cell types, the increased mitochondrial respiration underlies the longevity of
420 the cells. In our model we have not found most of the traditional markers used to define M2
421 alternative activation by flow cytometry at steady state (Supplemental Figure 1). Arg1 is the only
422 canonical M2 transcript that is modulated in the BMDM from infected male mice at steady state,
423 and that fold increase is relatively low (.894 log FC, adjusted *p*-value =.035). Arg1 drives the
424 production of polyamines, which in turn are able to modulate mitochondrial OxPHOS (Galvan-
425 Pena and O'Neill, 2014; Puleston et al., 2019). In the currently accepted paradigm of M2
426 polarization stat6 phosphorylation upregulates PGC1-β and PPARγ, leading to mitochondrial
427 biogenesis and increased beta-oxidation in addition to Arg1transcription. Here we present a
428 model where neither PGC1-β or PPARγ are modulated, but Arg1 transcription is increased with
429 a concomitant dramatic increase in mitochondrial respiration, suggesting that there may be
430 alternative ways to modulate mitochondrial metabolism.
431 Alternative activation has previously been shown to be dependent on cell intrinsic
432 lysosomal lipolysis and lal, with the defining feature being reductions in lipid droplets (Huang et
433 al., 2014). In our model using unstimulated BMDM from *S. mansoni* infected mice there is no
434 gross difference in lipid droplets, nor an increase in lal transcripts. Instead, we found a

435 significant shift in the lipidome of BMDM from infected male mice that centered on a reduction
436 in cholesterol esters. Previously published work in IL-4 induced M2 macrophages has found that
437 lipolysis centered on TGs as a fatty acid source. While we did find reductions in two species of
438 DGs and one species of monoacylglycerol (MG), there were no significant alterations to TAGs
439 in the BMDM generated from infected males. Flux analysis with heavy carbon labeled glucose
440 and palmitate suggest that BMDM from male infected mice have increased shuttling of both
441 glucose and palmitate into TCA cycle intermediates, suggesting that these cells have increased
442 mitochondrial beta oxidation. In addition to the unique lipidomic modulations, we found that the
443 dramatic increase in both basal oxygen consumption and spare respiratory capacity we observed
444 in BMDM from male infected mice was significantly palmitate dependent. This observation
445 further supports the idea that *in vivo* exposure of myeloid precursors to helminth antigens
446 induces unique metabolic modulations that focus on cholesterol and lipid metabolism as a source
447 for palmitate for beta oxidation. These data suggest that hybrid metabolic states in the absence of
448 M1 or M2 polarization occur in macrophages in the context of chronic disease, and present a
449 challenge to the dichotomy of M1 versus M2 activation being driven by immunometabolism.
450 Future studies exploring the immunometabolism of bone marrow derived and tissue resident
451 macrophages and dendritic cells from other chronic infections and inflammatory diseases are
452 needed in order to obtain a true picture of the correlation between metabolism and myeloid
453 polarization.

454 There are significant clinical differences in both the etiology and pathology of diabetes
455 and cardiovascular disease between males and females, but sex differences in immunological
456 activation or modulation by *S. mansoni* infection have not previously been studied in humans or
457 animal models. Surprisingly, we found that the unique metabolic modulations induced by *S.*

458 *mansoni* infection in BMDM from male mice do not occur in females, and infected females are
459 not reliably protected from high-fat diet induced obesity or glucose intolerance. Interestingly,
460 hepatic macrophage alternative activation in response to infection is equivalent between males
461 and females, but infection increases blood monocyte frequency in females to a much greater
462 extent than in males, suggesting sex specific modulation of either monopoiesis or monocyte
463 recruitment into tissues. Blood monocytes from infected males phenocopy the increase in
464 Mitotracker MFI that we have found in BMDM generated from infected males, indicating that
465 our BMDM model is likely an accurate representation of the *in vivo* potential of the myeloid
466 compartment. Interestingly, we found that infection significantly reduced the total number of
467 CMP and GMP in male, but not female bone marrow, again pointing to a sex-specific
468 modulation of the myeloid lineage at the precursor level. The reduction of CMP and GMP in
469 infected males suggests either an increase in the rate of differentiation into
470 monocytes/granulocytes, or decreased homeostatic proliferation. Since males have fewer blood
471 monocytes than female, we favor the later possibility. These possibilities and the relationship
472 between reductions in numbers of CMP and GMP in males, and the functional metabolic
473 differences in BMDM will be explored in future work.
474
475 Analysis of the BMDM transcriptomes from males and females revealed that over a
476 thousand genes are up regulated in male versus female BMDM regardless of *S. mansoni*
477 infection state. At the same time, over five dozen are differentially regulated by infection.
478 Focusing on the genes that are up-regulated in BMDM from infected males and down-regulated
479 in females, we found more than ten genes with known functions in cellular metabolism. Some of
480 these genes, like PFKFB3, have known regulatory elements for progesterone and estrogen (Shi et

481 al., 2017), but some of them, like fabp4, have no published mechanism of sex hormone
482 regulation. Glycolysis and cholesterol metabolism have previously been shown to directly affect
483 the inflammatory potential of myeloid cells. Our data indicate that *S. mansoni* infection induces a
484 hybrid inflammatory state in male but not female BMDM, where the LPS induced production of
485 nitrite and iNOS is enhanced, while the production of the key chronic pro-inflammatory
486 mediators IL-12p70, CXCL1, and IL-6 are reduced. This inflammatory profile is distinct from
487 what has previously been published with IL-4 induced M2 macrophages, where the production of
488 iNOS and nitrite are reduced following TLR stimulation (Lam et al., 2016). CXCL1 and IL-6
489 have previously been linked to increased monocyte recruitment and disease progression in both
490 atherosclerosis and obesity-induced diabetes (Boisvert et al., 2006; Hartman and Frishman, 2014;
491 Nunemaker et al., 2014; Qu et al., 2014; Zhou et al., 2011), so these data support the possibility
492 of infection driven modulation of macrophage function supporting the decreased pathology seen
493 in infected males. We have demonstrated that the modulation of macrophage oxygen
494 consumption is transferrable to an uninfected recipient, and can last for at least ten weeks,
495 suggesting that in males, *S. mansoni* infection induces long-lived metabolic modulation of the
496 myeloid lineage that survives in the absence of ongoing antigenic exposure. Trained innate
497 immunity has previously been documented to be induced by BCG immunization (Kaufmann et
498 al., 2018), and has recently been suggested to be the mechanism underlying the association
499 between previous bacterial and fungal infections and the development of atherosclerosis
500 (Hoogeveen et al., 2018; Leentjens et al., 2018). In these models, trained immunity and
501 epigenetic reprogramming is driven in part from a switch from oxidative phosphorylation to
502 increased aerobic glycolysis (Cheng et al., 2014; Stienstra et al., 2017). In the case of BCG,
503 trained circulating monocytes can be found months after immunization, which strongly suggests

504 reprogramming of bone marrow progenitors (Ifrim et al., 2014). Recent reports indicate that
505 western high-fat diet itself also induces innate training of bone marrow progenitors in both the
506 $Ldr^{-/-}$ model of atherosclerosis (Christ et al., 2018) and in obesity related steatohepatitis (Krenkel
507 et al., 2020). Our data suggests that *S. mansoni* infection in males trains the myeloid lineage in
508 the opposite fashion; modulating the metabolic transcriptome of the myeloid lineage such that
509 oxidative phosphorylation and mitochondrial activity is increased, while the chronic
510 inflammatory potential is decreased. Alterations to the numbers and frequency of myeloid
511 progenitors and the transferability of our phenotype via bone marrow suggests that progenitors
512 are indeed modulated in our model, the relative role of epigenetic modulation versus microRNA
513 regulation in dictating the *S. mansoni* induced myeloid transcriptome will be the subject of future
514 studies.

515 There are significant differences in both the susceptibility and disease presentation
516 between males and females for both diabetes and cardiovascular disease, but few studies have
517 focused on the role of immunometabolism in this dichotomy. Our data suggests apparent
518 biological sex-dependent differences in both the ability of schistosomes to protect from the
519 development of HFD induced metabolic disease parameters, and the ability to modulate
520 macrophage glucose and lipid metabolism. The current epidemiological data strongly indicates
521 an inverse correlation between helminth infections and metabolic diseases such as diabetes and
522 cardiovascular disease, but these studies were not designed to identify sex-specific correlations.
523 Few animal studies have focused on the role of myeloid cells in driving sex-specific metabolic
524 differences. Our current data indicate a clear need for further studies in both humans and animal
525 models to specifically probe the relationship between biological sex and myeloid metabolism,
526 and how chronic helminth infections modulate this.

527

528 **Conflict of Interest**

529 The authors declare no competing interests.

530 **Acknowledgements**

531 The work was supported by The University of Utah, a Scientist Development Grant from the

532 American Heart Association to KCF (14SDG18230012), an American Heart Association Pre-

533 doctoral Award (18PRE34030086) to DCS, and 1R21AI135385-01A1 to EA. *B. glabrata* snails

534 provided by the NIAID Schistosomiasis Resource Center of the Biomedical Research Institute

535 (Rockville, MD) through NIH-NIAID Contract HHSN272201700014I for distribution through

536 BEI Resources. JEC is supported through U54 DK110858-01, mass spectrometry equipment

537 employed was provided by 1S10OD016232-01, 1S10OD018210-01A1 and 1S10OD021505-01

538 to JEC.

539

540 **STAR Methods**

541 **KEY RESOURCES TABLE**

REAGENT or RESOURCE	SOURCE	IDENTIFIER
Antibodies		
Anti-mouse F4/80 (Clone: BM8)	Biolegend	Cat no. 123114
Anti-mouse CD64 a and b Alloantigens (Clone: X54-5/7.1.1)	BD Biosciences	Cat no. 558455
Biotinylated Goat Anti-m-Mer	R&D Systems	Cat no. BAF591
Anti-mouse CD11c (Clone: N418)	BioLegend	Cat no. 117306
Rat Anti-mouse I-A/I-E (Clone: M5/114.15.2)	BD Biosciences	Cat no. 562366
Anti-mouse Ly6A/E (Sca-1) (Clone: D7)	eBiosciences	Cat no.17-5981-82
Rat anti-mouse CD117/c-kit	R&D Systems	Cat no. FAB1356
Anti-mouse CD115 (Clone: AFS98)	eBiosciences	Cat no. 25-1152-82
Anti-mouse CD16/32 (Clone: 93)	Invitrogen	Cat no.25-0161-82
Anti-mouse CD4 (Clone: GK1.5)	BioLegend	Cat no.100406
Anti-mouse CD206 (Clone:C06C2)	BioLegend	Cat no. 141721
Rat Anti-mouse CD301	BioRad	Cat no. MCA2392A488
Anti-mouse Nos2 (Clone: CXNFT)	Invitrogen	Cat no. 46-5920-80

Anti Hu/Mo Arg1 (Clone: A1exF5)	Invitrogen	Cat no.48-3697-80
Anti-mouse CD19 (Clone: MB19-1)	Invitrogen	Cat no.11-0191-85
Anti-mouse Ter119 (Clone: Ter-119)	Invitrogen	Cat no. 11-5921082
Rat Anti-mouse Ly6G and Ly6C (Clone: RB6-8C5)	BD Biosciences	Cat no. 553127
Anti-mouse CD3 (Clone: 17A2)	BioLegend	Cat no. 100204
Anti-mouse Ly6C (Clone: HK1.4)	Invitrogen	Cat no. 45-5932-82
Anti-mouse CD45 (Clone 30-F11)	Biolegend	Cat no.103154
Anti-mouse CD11b (Clone: M1/70)	eBiosciences	Cat no. 56-0112-82
MitoTracker™ Deep Red FM	Invitrogen	Cat no. M22426
Anti-mouse CD34 (Clone: SA376A4)	BioLegend	Cat no.152203
TrueStain fcX (anti-mouse CD16/32) (Clone: 93)	BioLegend	Cat no.101320
Anti-mouse CD127 (Clone: A7R34)	BioLegend	Cat no. 135043
Biological Samples		
Fetal Bovine Serum	ThermoFisher	Cat no. 10091148
Chemicals, Peptides, and Recombinant Proteins		
Endotoxin free LPS (Escherichia coli Serotype O)	InvivoGen	Cat no. tlrl-eblps
D-Glucose-^{13}C6	Sigma Aldrich	Cat no. 389374
Recombinant murine M-CSF	Peprotech	Cat no. 315-03
BD Pharm Lyse Lysing Buffer	BD Biosciences	Cat no. 555899
Taqman Gene Expression Master Mix	Applied Biosystems	Cat no.4369016
Trypan Blue solution	Sigma	T81154-100ML
Streptavidin APC	BD Biosciences	Cat no. 554067
Streptavidin APC/Fire 750	Biolegend	Cat no.405250
Streptavidin PE	BD Biosciences	Cat no. 554061
Streptavidin PB	Invitrogen	Cat no. S11222
Streptavidin PE-Cy5	BD Biosciences	Cat no. 554062
(Ethylenedinitrilo)tetraacetic acid (EDTA)	Thermo Fisher Scientific	Cat no. AM9260G
Fixation/Permeabilization		
Collagenase	Sigma Aldrich	Cat no. 5138
Trizol LS Reagent	Ambion	Cat no. 10296028
Chloroform	Alfa Aesar	Cat no. 32614
Glucose	Sigma Aldrich	Cat no. G7528
2-Propanol	Fisher Chemical	Cat no. A416
Critical Commercial Assays		
Seahorse Bioassay	Agilent Technologies	Cat no.102416
SuperScript IV-VILO Master Mix	Thermo Fisher	Cat no.11766050
RNA Clean and Concentrator Kit	Zymo Research	Cat no. 11-353
Zombie Red Fixable Viability Kit	BioLegend	Cat no.423109
^{13}C Glucose	Santa Cruz Biotech	Cat no. 106032-62-6
^{13}C Palmitate	Sigma-Aldrich	Cat no. 605573
Cellstripper cell dissociation reagent	Corning	Cat no. 25-056-CI

Western High-fat diet	Envigo	TD 88137
Deposited Data		
GEO	https://www.ncbi.nlm.nih.gov/geo/	GSE144447
Experimental Models: Organisms/Strains		
B6.129P2-Apoetm1Unc/J	The Jackson Laboratory	Stock No: 002052
Parasite: *Schistosoma mansoni*	Biomedical Research Institute	https://www.afbr-bri.org/schistosomiasis/ordering/
Software and Algorithms		
FlowJo Software X 10.0.7r2	BD Biosciences	https://www.flowjo.com/solutions/flowjo/downloads/previous-versions
GraphPad Prism 8.2.0	GraphPad	https://www.graphpad.com/support/faq/prism-820-release-notes/
Attune NxT Accoustic Focusing Cytometer	Invitrogen	https://www.thermofisher.com/us/en/home/life-science/cell-analysis/flow-cytometry/flow-cytometers/attune-acoustic-focusing-flow-cytometer.html
iPathways Guide	Advaita	https://advaitabio.com/ipathwayguide/
MH Qual	Agilent Technologies, Inc	https://www.agilent.com/en/products/software-informatics/masshunter-suite/masshunter/masshunter-software
MassHunter Quantitative Analysis B.07.00	Agilent Technologies, Inc	https://www.agilent.com/en/products/software-informatics/masshunter-suite/masshunter/masshunter-software
LipidMatch	University of Florida	http://secim.ufl.edu/secim-tools/lipidmatch/
MetaboAnalyst 3.0	Xia et al., 2015	http://www.metaboanalyst.ca
Other		

Mgll Taqman Gene Expression Assay	ThermoFisher	Assay ID: Mm00449274_m1
Slc1a3 Taqman Gene Expression Assay	ThermoFisher	Assay ID: Mm00600697_m1.
Beta actin Taqman Gene Expression Assay	ThermoFisher	Assay ID: Mm00607939_s1

542

543 **LEAD CONTACT AND MATERIALS AVAILABILITY**

544 Further information requests should be directed to and will be fulfilled by the Lead Contact,

545 Keke Fairfax (keke.fairfax@path.utah.edu). These studies generated no new reagents.

546

547 **EXPERIMENTAL MODEL AND SUBJECT DETAILS**

548 **Parasite and Mouse Models**

549 This study was carried out in accordance with the recommendations in the Guide for the Care

550 and Use of Laboratory Animals of the National Institutes of Health. The protocols were

551 approved by the Institutional Animal Care and Use Committees of the University of Utah and

552 Purdue University. Snails infected with *S. mansoni* (strain NMRI, NR-21962) were provided by

553 the Schistosome Research Reagent Resource Center for distribution by BEI Resources, NIAID

554 NIH. Male and female ApoE$^{-/-}$ (B6.129P2-Apoetm1Unc/J) were purchased from the Jackson

555 Laboratories and bred at the University of Utah. Mice were housed in pathogen-free conditions

556 and were fed standard rodent chow (2019 rodent chow, Harlan Teklad) until 10-14 days before

557 infection when they were transitioned to a high-fat diet (HFD: 21% milk fat, 0.15% cholesterol:

558 TD 88137 Envigo). Bone marrow chimeras were generated by treating ApoE$^{-/-}$ mice that had

559 been on high- fat diet for 4 weeks with 20mg/kg of pharmaceutical grade busulfan for 5 days

560 (total dose of 100mg/kg). On day 6 mice were i.v. injected with 2.5-3 x 10^6 bone marrow cells

561 from either 10-week *S. mansoni* infected or control uninfected ApoE$^{-/-}$ mice on high-fat diet.

562 Reconstitution was validated via flow-cytometry at 3-weeks post-transfer and recipient mice
563 were maintained on high-fat diet for 10-weeks post-reconstitution.

564 **METHOD DETAILS**

565 ***S. mansoni* infection and glucose tolerance test**

566 ApoE$^{-/-}$ female and male mice of 6 weeks of age were exposed percutaneously to 75-90 cercariae
567 of *S. mansoni* or were mocked infected (as controls). At five- and ten-weeks post-infection mice
568 were fasted for 5 hours and baseline blood glucose levels were obtained via lateral tail vein nick.
569 Mice were then administered a single intraperitoneal injection of glucose (2mg/g of body weight,
570 ultrapure glucose, Sigma G7528). Blood glucose levels were obtained at 20, 60, and 90 min post
571 injection. Individual data points obtained were analyzed by Area Under Curve (AUC).

572

573 **Mouse macrophage culture**

574 Mouse bone marrow-derived macrophages (BMDM) were generated as follows: bone marrow
575 cells were isolated by centrifugation of bones at >10,000 x g in a microcentrifuge tube for 15
576 seconds as previously described (Amend et al., 2016). Cells were differentiated in M-CSF
577 (20ng/mL, Peprotech, Rocky Hill, NJ) in complete macrophage medium (CMM: RPMI1640,
578 10% FCS, 2mM L-glutamine and 1 IU/mL Pen-Strep for 6 or 7 days. On the last day, cells
579 were harvested in Cellstripper cell dissociation reagent (Corning) were washed with CMM) and
580 prepared for downstream assays.

581

582 **Glycolytic and phospho-oxidative metabolism measurement (seahorse assay)**

583 BMDM from different conditions (uninfected controls or *S. mansoni* infected) were resuspended
584 at the same concentration in XF assay media supplemented with 5% FCS and 5mM glucose. The

585 day before the assay, the probe plate was calibrated and incubated at 37 C in a non-CO2
586 incubator. Resuspended cells were seeded at a concentration of $1.5x10^5$ cells per well and
587 incubated for 20-60 minutes in the Prep Station incubator (37 C non-CO2 incubator). Following
588 initial incubation, XF Running Media (XF assay media with 5% FCS and 10mM Glucose) were
589 dispensed into each well. OCR and ECAR were measured by an XF96 Seahorse Extracellular
590 Flux Analyzer following the manufacturer's instructions. For the seahorse assay, cells were
591 treated with oligomycin (1uM), FCCP (1.5uM), rotenone (100nM) and antimycin A (1uM). Each
592 condition was performed in 2-3 technical replicates. For determination of palmitate dependent
593 respiration, BSA-conjugated palmitate (BSA: palmitate = 1:6, molar ratio) was prepared
594 according to the Seahorse protocol (Seahorse Bioscience). Briefly, 1 mM sodium palmitate
595 (Sigma Aldrich) was conjugated with 0.17 mM fatty acid free-BSA (Sigma Aldrich) in 150 mM
596 NaCl solution at 37°C for 1h. Palmitate-BSA was stored in glass vials at -20°C until use. Cells
597 were incubated as above in glucose limited XF media per manufacturer instructions.
598
599 **Flow Cytometry**
600 Livers from uninfected and infected mice were perfused with 1X PBS, mashed and digested in
601 DMEM 0.5% Collagenase (Sigma) at 37°C for 15 min. Then, livers were mashed and filtered
602 through a 100 µm metal strainer and digested an additional 15 min. Following second digestion,
603 the liver contents were strained, washed with DMEM and spun down 1500 rpm for 5 min. The
604 pellet was lysed with 1X lysis buffer (BD PharmLyse), quenched with 1% FBS DMEM, and
605 washed to be used in flow cytometry. Surface staining was performed using the following mAb
606 against mouse antigens: CD45 (30-F11, eBioscience), CD301(BioRad), CD206 (C068C2,
607 Biolegend), F4/80 (BM8, Biolegend), mouse Mer biotinylated (R&D), CD64(X54-5/7.1, BD).

608 Intracellular antigen staining such as Nos2 (CXNFT, Invitrogen, and C-11, Santa Cruz) and Arg1
609 (Invitrogen, A1exF5)) was performed using the Intracellular Fixation and Permeabilization
610 Buffer set (Thermo Fisher Scientific cat. no. 88-8824) per manufacturer's instruction. Further,
611 bone marrow cells were obtained by centrifugation of bones into tubes at >10000 rpm for 15 s.
612 Surface staining for bone marrow precursors was performed using the following antibodies:
613 Ter119, CD19, CD4, CD3, Gr-1, CD11b, Sca-1, CD115, Ly6C, c-Kit, flt3, CD127 and CD16/32.
614 PBMC from whole blood were obtained following red blood cell lysis and used for flow
615 cytometry analysis. Surface staining of PBMC was performed using Ter119, CD64, CD11b,
616 CD115, Ly6C and MitoTracker Red.
617 Samples were acquired using Attune NxT Focusing Flow Cytometer (Thermo Fisher Scientific)
618 and analyzed using Flowjo X 10.0.7r2 (FlowJo LLC, Inc.).
619
620 **RNA Isolation and q-RT-PCR**
621 BMDM were stored in Trizol, and RNA isolation was performed as described in the
622 Immunological Genome Project Total RNA isolation protocol. Next, cDNA was synthesized
623 from RNA using Superscript IV VILO (ThermoFisher Scientific) for reverse transcription. qPCR
624 was performed using TaqMan Gene expression assays (Mgll, Slc1a3, beta actin, ThermoFisher)
625 on an Applied Biosystems Stepone Plus Real-Time PCR System. Beta-Actin assay number
626 Mm00607939_s1, mgll assay Mm00449274_m1, slc1a3 assay Mm00600697_m1. Relative
627 expression was calculated using the 2-ΔΔCt method.
628
629 **Measurement of Cytokines and Inflammatory mediators**

630 For cytokine levels of BMDCs, supernatants were collected at 24 hours post stimulation and
631 measured with Mouse Cytokine and Chemokine ProcartaPlex 26plex panel (Life Technologies)
632 per manufacture instructions using a Luminex Magpix system. Nitrite levels in cell culture media
633 were determined using a Griess reagent kit for nitrite determination (Invitrogen) according the
634 manufacturer's instructions.
635
636 **Untargeted lipidomics**
637 *Sample extraction from serum or cell pellets*
638 Lipids were extracted from serum (50µL) or cell pellets in a combined solution as described in
639 (Matyash et al., 2008). In detail, samples were combined in solution with 225 µL MeOH
640 containing internal standards (IS; Avanti splash Lipidomix (Lot#12), 10µL each sample) and 750
641 µL methyl tert-butyl ether (MTBE). The samples were sonicated for 1 min, rested on ice for 1
642 hour, briefly vortexed every 15 min then an addition of 200µL dd-H2O was made to induce
643 phase separation. All solutions were pre-chilled on ice. The sample were then vortexed for 20 s,
644 rested at room temperature for 10 min, and centrifuged at 14,000 g for 10 min at 4 C. The upper
645 organic phase was collected and evaporated to dryness under vacuum. Lipid samples were
646 reconstituted in 200µL IPA and transferred to an LC-MS vial with insert for analysis.
647 Concurrently, a process blank sample was brought forward as well as quality control sample was
648 prepared by taking equal volumes (10µL per sample) from each sample after final resuspension.
649
650 *LC-MS Methods*
651 Lipid extracts were separated on a Waters Acquity UPLC CSH C18 1.7 um 2.1 x 100 mm
652 column maintained at 65 °C connected to an Agilent HiP 1290 Sampler, Agilent 1290 Infinity

653 pump, equipped with an Agilent 1290 Flex Cube and Agilent 6530 Accurate Mass Q-TOF dual
654 ESI mass spectrometer. For positive mode, the source gas temperature was set to 225 °C, with a
655 gas flow of 11 L/min and a nebulizer pressure of 50 psig. VCap voltage was set at 3500 V,
656 fragmentor at 110 V, skimmer at 85 V and Octopole RF peak at 750 V. For negative mode, the
657 source gas temperature was set at 325 °C, with a drying gas flow of 12 L/min and a nebulizer
658 pressure of 30 psig. VCap voltage is set 3000 V, fragmentor at125 V, skimmer at 75 V and
659 Octopole RF peak at 750 V. Reference masses in positive mode (*m/z* 121.0509 and 922.0098)
660 were infused with nebulizer pressure at 2 psig, in negative mode reference masses (*m/z*
661 1033.988, 966.0007, 112.9856 and 68.9958) were infused with a nebulizer pressure at 5psig.
662 Samples were analyzed in a randomized order in both positive and negative ionization modes in
663 separate experiments acquiring with the scan range m/z 100-1700. Mobile phase A consisted of
664 ACN:H_2O (60:40 *v/v*) in 10 mM ammonium formate and 0.1% formic acid, and mobile phase B
665 consisted of IPA:ACN:H_20 (90:9:1 *v/v*) in 10 mM ammonium formate and 0.1% formic acid.
666 The chromatography gradient for both positive and negative modes started at 15% mobile phase
667 B then increased to 30% B over 2.4 min, then increased to 48% from 2.4-3.0 min, followed by an
668 increase to 82% B from 3-13.2 min, and then to 99% from 13.2-13.8 min where it was held until
669 15.4 min and then returned to the initial conditioned and equilibrated for 4 min. Flow was 0.5
670 mL/min throughout, injection volume was 5μL for positive and 7 μL negative mode. Tandem
671 mass spectrometry is conducted using the same LC gradient at collision energies of 20 V and 40
672 V.
673
674 **Targeted lipidomics**
675 *Sample Preparation*

676 Lipids were extracted from cell pellets (500,000 cells) as described in detail above (Matyash et
677 al., 2008). For targeted lipidomics, lipid extracts were separated on a Waters BEH HILIC column
678 1.7 µm, 100 mm × 3 mm column maintained at 60 °C connected to an Agilent HiP 1290
679 Sampler, Agilent 1290 Infinity pump, and equipped with an Agilent 6490 triple quadrupole
680 (QqQ) mass spectrometer. Lipids were detected using dynamic multiple reaction monitoring
681 (dMRM) in negative ion mode. Source gas temperature is set to 225 °C, with a gas flow of 13
682 L/min and a nebulizer pressure of 30 psi. Sheath gas temperature was 350 °C, sheath gas flow
683 was 11 L/min, capillary voltage of 4000 V, nozzle voltage was 500 V, high pressure RF was 190
684 V and low-pressure RF was 120 V. Injection volume was 2 µL and the samples were injected in
685 a randomized order. Mobile phase A consisted of H_2O, mobile phase B consisted of ACN:H_2O
686 (96:4 *v/v*) and both contain 7 mM ammonium acetate. The chromatography gradient started at
687 100% mobile phase B and decreased to 84% B over 10 min. Post-time was 9 min and the flow
688 rate was 0.4 mL/min throughout. Collision energies (25 V) and cell accelerator voltages (3 V)
689 were optimized using lipid standards with dMRM quantifier transitions as $[M-H]^- \rightarrow [T2_RCOO]^-$
690 and qualifier transitions of $[M-H]^- \rightarrow [T1_RCOO]^-$ and $[M-H]^- \rightarrow [NL_T2Ketene]^-$.
691
692 **Lipid data analysis**
693 The pooled QC samples and process blank samples were injected throughout the sample queue to
694 ensure the reliability of acquired LC-MS data. Results from LC-MS experiments were collected
695 using Agilent MassHunter (MH) Workstation and analyzed using the software packages MH
696 Qual, MH Quant (Agilent Technologies, Inc) and LipidMatch to prepare the data set.
697 The data table exported from MHQuant was evaluated using Excel where initial lipid targets
698 were parsed based on the following criteria. Only lipids with relative standard deviation (RSD)

699 less than 30% in QC samples were used for data analysis. Additionally, targets identified in
700 blanks or double blanks at significant amounts (area under the curve (AUC) target blank/AUC
701 target QC >30%) were removed from analysis. Lipids were quantitated based on peak area ratios
702 to the spiked IS of the same or nearest class.
703
704 **RNA Sequencing**
705 Library Preparation and sequencing
706 The concentration and quality of total RNA samples was first assessed using Agilent 2100
707 Bioanalyzer. A RIN (RNA Integrity Number) of five or higher was required to pass the quality
708 control. Then 200 nanograms of RNA per sample were used to prepared dual-indexed strand-
709 specific cDNA library using KAPA mRNA Hyperprep Kit (Roche). The resulting libraries were
710 assessed for its quantity and size distribution using Qubit and Agilent 2100 Bioanalyzer. Two
711 hundred pico molar pooled libraries were utilized per flowcell for clustering amplification on
712 cBot using HiSeq 3000/4000 PE Cluster Kit and sequenced with 2.75bp paired-end configuration
713 on HiSeq4000 (Illumina) using HiSeq 3000/4000 PE SBS Kit. A Phred quality score (Q score)
714 was used to measure the quality of sequencing. More than 90% of the sequencing reads reached
715 Q30 (99.9% base call accuracy).
716
717 Sequence alignment and gene counts
718 The sequencing data were first assessed using FastQC (Babraham Bioinformatics, Cambridge,
719 UK) for quality control. Then all sequenced libraries were mapped to the mouse genome (UCSC
720 mm10) using STAR RNA-seq aligner (Dobin et al., 2013) with the following parameter: "--
721 outSAMmapqUnique 60". The reads distribution across the genome was assessed using bamutils

722 (from ngsutils) (Breese and Liu, 2013). Uniquely mapped sequencing reads were assigned to
723 mm10 refGene genes using featureCounts (from subread) (Liao et al., 2014) with the following
724 parameters: "-s 2 –p –Q 10". Quality control of sequencing and mapping results was summarized
725 using MultiQC (Ewels et al., 2016). Genes with read count per million (CPM) > 0.5 in more than
726 2 of the samples were kept. The data was normalized using TMM (trimmed mean of M values)
727 method. Differential expression analysis was performed using edgeR (McCarthy et al., 2012;
728 Robinson et al., 2010). False discovery rate (FDR) was computed from p-values using the
729 Benjamini-Hochberg procedure.
730 Pathway analysis
731 The Data (significantly impacted pathways, biological processes, molecular interactions.) were
732 analyzed using Advaita Bio's iPathwayGuide (http://www.advaitabio.com/ipathwayguide).
733 Pathway analysis was performed on log_2-transformed data using Bonferroni-corrected *p*-values.
734 The data discussed in this publication have been deposited in NCBI's Gene Expression Omnibus
735 (Edgar *et al*., 2002) and are accessible through GEO Series accession number GSE
736 144447(https://www.ncbi.nlm.nih.gov/geo/query/acc.cgi?acc=GSE144447)
737
738 **Heavy glucose and heavy palmitate labeling**
739 For metabolomics tracing in Figure 2 BMDM were differentiated in CMM containing normal
740 glucose. At Day 6 of culture cells were switched to CMM containing $^{13}C_6$-glucose (Santa Cruz
741 Biotech) for 24 hours. Cells were harvested and processed as described below. For metabolomics
742 tracing in figure 5 BMDM were differentiated in CMM containing normal glucose and serum. At
743 Day 6 of culture cells were switched to CMM containing dialyzed serum and 1 mM ^{13}C
744 palmitate (sigma Aldrich) for 36 hours. Cells were harvested and processed as described below.

745
746

747 **Metabolomics**

748 *Extraction*

749 Cold 90% methanol (MeOH) solution was added to each sample to give a final concentration of
750 80% MeOH to each cell pellet. Samples were incubated at -20 °C for 1 hr. After incubation, the
751 samples were centrifuged at 20,000 x g for 10 minutes at 4 °C. The supernatant was transferred
752 from each sample tube into a labeled, fresh micro centrifuge tube. The samples were dried *en*
753 *vacuo*.

754

755 *Mass Spectrometry Analysis of Samples*

756 All GC-MS analysis was performed with an Agilent 7200 GC-QTOF and an Agilent 7693A
757 automatic liquid sampler. Dried samples were suspended in 40 µL of a 40 mg/mL O-
758 methoxylamine hydrochloride (MOX) (MP Bio #155405) in dry pyridine (EMD Millipore
759 #PX2012-7) and incubated for one hour at 37 °C in a sand bath. 25 µL of this solution was
760 added to auto sampler vials followed by the automatic addition of 60 µL of N-methyl-N-
761 trimethylsilyltrifluoracetamide (MSTFA with 1%TMCS, Thermo #TS48913) and incubated for
762 30 minutes at 37 °C. Following incubation, each sample were vortexed and 1 µL of the prepared
763 sample was injected into the gas chromatograph inlet in the split mode with the inlet temperature
764 held at 250 °C. A 10:1 split ratio was used for analysis for the majority of metabolites. Any
765 metabolites that saturated the instrument at the 10:1 split was analyzed at a 50:1 split ratio. The
766 gas chromatograph had an initial temperature of 60 °C for one minute followed by a 10°C/min
767 ramp to 325 °C and a hold time of 10 minutes. A 30-meter Agilent Zorbax DB-5MS with 10 m

768 Duraguard capillary column was employed for chromatographic separation. Helium was used as
769 the carrier gas at a rate of 1 mL/min.
770
771 *Data Analysis*
772 The area under the curve for each isotope was extracted using MHQuant software (Agilent). This
773 data was exported as a .csv file and isotopically corrected using an in house modified version of
774 DeuteRater (Naylor et al., 2017)
775
776 **Machine Learning**
777 The selection of the most informative or important features (i.e., the features contributing to the
778 prediction) was performed using a machine-learning approach involving an elastic-net regressor,
779 which followed a round of traditional univariate filtering. The process included two steps:
780 1. Creating a series of ANOVA models (one for each of the lipid-based features), and pre-
781 selecting features based on η^2 to limit the complexity of the downstream elastic net
782 model. The uninformative features were rejected and not used in the second step.
783 2. Establishing an elastic net regression model via cross-validation and grid-search of the
784 parameters. The zero coefficients of the model were removed. The top 20 non-zero
785 coefficients provided ranking for the features in terms of their importance.

786 The elastic net regression attempts to minimize the following functional:

787 $$\hat{\beta} = \underset{\beta}{\operatorname{argmin}}\left(\left|\left|y - X\beta\right|\right|^2 + \lambda\left(\left(1-\alpha\right)\left|\left|\beta\right|\right|^2 / 2 + \alpha\left|\left|\beta\right|\right|_1\right)\right)$$

788 over a grid of α and λ values (Zou, 2005). The elastic-net approach linearly combines the L_1 and
789 L_2 penalties used in LASSO (Tibshirani, 1996) and ridge-regression methods (Hoerl, 1970),

respectively. Therefore, the elastic net penalty would become LASSO penalty for $\alpha = 1$ and ridge penalty for $\alpha = 0$. The parameter λ controls the overall strength of the combined penalty term. The input X in the model consists of all the molecular features identified, and y is probability of observing a particular animal.

Statistical Analysis

Statistical analyses of data were performed using one-way ANOVA, a non-parametric Mann-Whitney test, or unpaired Student's t-test depending on the data distribution. $P \leq 0.05$ were considered statistically significant. Analyses and graphing were performed using Prism (GraphPad v8.0) and R-language for statistical computing.

References

Amend, S.R., Valkenburg, K.C., and Pienta, K.J. (2016). Murine Hind Limb Long Bone Dissection and Bone Marrow Isolation. J Vis Exp.

Anheuser, S., Breiden, B., and Sandhoff, K. (2019). Membrane lipids and their degradation compounds control GM2 catabolism at intralysosomal luminal vesicles. J Lipid Res *60*, 1099-1111.

Baars, A., Oosting, A., Lohuis, M., Koehorst, M., El Aidy, S., Hugenholtz, F., Smidt, H., Mischke, M., Boekschoten, M.V., Verkade, H.J., et al. (2018). Sex differences in lipid metabolism are affected by presence of the gut microbiota. Sci Rep *8*, 13426.

Barron, L., and Wynn, T.A. (2011). Macrophage activation governs schistosomiasis-induced inflammation and fibrosis. European journal of immunology *41*, 2509-2514.

Beliard, S., Le Goff, W., Saint-Charles, F., Poupel, L., Deswaerte, V., Bouchareychas, L., Huby, T., and Lesnik, P. (2017). Modulation of Gr1(low) monocyte subset impacts insulin sensitivity and weight gain upon high-fat diet in female mice. Int J Obes (Lond) *41*, 1805-1814.

Berdan, C.A., Erion, K.A., Burritt, N.E., Corkey, B.E., and Deeney, J.T. (2016). Inhibition of Monoacylglycerol Lipase Activity Decreases Glucose-Stimulated Insulin Secretion in INS-1 (832/13) Cells and Rat Islets. PloS one *11*, e0149008.

Boisvert, W.A., Rose, D.M., Johnson, K.A., Fuentes, M.E., Lira, S.A., Curtiss, L.K., and Terkeltaub, R.A. (2006). Up-regulated expression of the CXCR2 ligand KC/GRO-alpha in atherosclerotic

822 lesions plays a central role in macrophage accumulation and lesion progression. The American
823 journal of pathology *168*, 1385-1395.
824 Breese, M.R., and Liu, Y. (2013). NGSUtils: a software suite for analyzing and manipulating next-
825 generation sequencing datasets. Bioinformatics *29*, 494-496.
826 Carroll, R.G., Zaslona, Z., Galvan-Pena, S., Koppe, E.L., Sevin, D.C., Angiari, S., Triantafilou, M.,
827 Triantafilou, K., Modis, L.K., and O'Neill, L.A. (2018). An unexpected link between fatty acid
828 synthase and cholesterol synthesis in proinflammatory macrophage activation. The Journal of
829 biological chemistry *293*, 5509-5521.
830 Chella Krishnan, K., Mehrabian, M., and Lusis, A.J. (2018). Sex differences in metabolism and
831 cardiometabolic disorders. Curr Opin Lipidol *29*, 404-410.
832 Chen, Y., Lu, J., Huang, Y., Wang, T., Xu, Y., Xu, M., Li, M., Wang, W., Li, D., Bi, Y., et al. (2013).
833 Association of previous schistosome infection with diabetes and metabolic syndrome: a cross-
834 sectional study in rural China. The Journal of clinical endocrinology and metabolism *98*, E283-
835 287.
836 Cheng, S.C., Quintin, J., Cramer, R.A., Shepardson, K.M., Saeed, S., Kumar, V., Giamarellos-
837 Bourboulis, E.J., Martens, J.H., Rao, N.A., Aghajanirefah, A., et al. (2014). mTOR- and HIF-1alpha-
838 mediated aerobic glycolysis as metabolic basis for trained immunity. Science *345*, 1250684.
839 Christ, A., Gunther, P., Lauterbach, M.A.R., Duewell, P., Biswas, D., Pelka, K., Scholz, C.J.,
840 Oosting, M., Haendler, K., Bassler, K., et al. (2018). Western Diet Triggers NLRP3-Dependent
841 Innate Immune Reprogramming. Cell *172*, 162-175 e114.
842 Cnop, M., Havel, P.J., Utzschneider, K.M., Carr, D.B., Sinha, M.K., Boyko, E.J., Retzlaff, B.M.,
843 Knopp, R.H., Brunzell, J.D., and Kahn, S.E. (2003). Relationship of adiponectin to body fat
844 distribution, insulin sensitivity and plasma lipoproteins: evidence for independent roles of age
845 and sex. Diabetologia *46*, 459-469.
846 Cortes-Selva, D., Elvington, A.F., Ready, A., Rajwa, B., Pearce, E.J., Randolph, G.J., and Fairfax,
847 K.C. (2018). Schistosoma mansoni Infection-Induced Transcriptional Changes in Hepatic
848 Macrophage Metabolism Correlate With an Athero-Protective Phenotype. Front Immunol *9*,
849 2580.
850 Dobin, A., Davis, C.A., Schlesinger, F., Drenkow, J., Zaleski, C., Jha, S., Batut, P., Chaisson, M.,
851 and Gingeras, T.R. (2013). STAR: ultrafast universal RNA-seq aligner. Bioinformatics *29*, 15-21.
852 Doenhoff, M.J., Stanley, R.G., Griffiths, K., and Jackson, C.L. (2002). An anti-atherogenic effect of
853 Schistosoma mansoni infections in mice associated with a parasite-induced lowering of blood
854 total cholesterol. Parasitology *125*, 415-421.
855 Douglass, J.D., Zhou, Y.X., Wu, A., Zadroga, J.A., Gajda, A.M., Lackey, A.I., Lang, W., Chevalier,
856 K.M., Sutton, S.W., Zhang, S.P., et al. (2015). Global deletion of MGL in mice delays lipid
857 absorption and alters energy homeostasis and diet-induced obesity. J Lipid Res *56*, 1153-1171.
858 Emerging Risk Factors, C., Sarwar, N., Gao, P., Seshasai, S.R., Gobin, R., Kaptoge, S., Di
859 Angelantonio, E., Ingelsson, E., Lawlor, D.A., Selvin, E., et al. (2010). Diabetes mellitus, fasting
860 blood glucose concentration, and risk of vascular disease: a collaborative meta-analysis of 102
861 prospective studies. Lancet *375*, 2215-2222.
862 Ewels, P., Magnusson, M., Lundin, S., and Kaller, M. (2016). MultiQC: summarize analysis results
863 for multiple tools and samples in a single report. Bioinformatics *32*, 3047-3048.

Fairfax, K.C., Amiel, E., King, I.L., Freitas, T.C., Mohrs, M., and Pearce, E.J. (2012). IL-10R blockade during chronic schistosomiasis mansoni results in the loss of B cells from the liver and the development of severe pulmonary disease. PLoS pathogens *8*, e1002490.
Funk, J.L., Feingold, K.R., Moser, A.H., and Grunfeld, C. (1993). Lipopolysaccharide stimulation of RAW 264.7 macrophages induces lipid accumulation and foam cell formation. Atherosclerosis *98*, 67-82.
Galvan-Pena, S., and O'Neill, L.A. (2014). Metabolic reprograming in macrophage polarization. Front Immunol *5*, 420.
Garaude, J., Acin-Perez, R., Martinez-Cano, S., Enamorado, M., Ugolini, M., Nistal-Villan, E., Hervas-Stubbs, S., Pelegrin, P., Sander, L.E., Enriquez, J.A., et al. (2016). Mitochondrial respiratory-chain adaptations in macrophages contribute to antibacterial host defense. Nature immunology *17*, 1037-1045.
Girgis, N.M., Gundra, U.M., Ward, L.N., Cabrera, M., Frevert, U., and Loke, P. (2014). Ly6C(high) monocytes become alternatively activated macrophages in schistosome granulomas with help from CD4+ cells. PLoS pathogens *10*, e1004080.
Griffin, C., Lanzetta, N., Eter, L., and Singer, K. (2016). Sexually dimorphic myeloid inflammatory and metabolic responses to diet-induced obesity. American journal of physiology. Regulatory, integrative and comparative physiology *311*, R211-216.
Hartman, J., and Frishman, W.H. (2014). Inflammation and atherosclerosis: a review of the role of interleukin-6 in the development of atherosclerosis and the potential for targeted drug therapy. Cardiol Rev *22*, 147-151.
Herbert, D.R., Holscher, C., Mohrs, M., Arendse, B., Schwegmann, A., Radwanska, M., Leeto, M., Kirsch, R., Hall, P., Mossmann, H., et al. (2004). Alternative macrophage activation is essential for survival during schistosomiasis and downmodulates T helper 1 responses and immunopathology. Immunity *20*, 623-635.
Hinton, W., McGovern, A., Coyle, R., Han, T.S., Sharma, P., Correa, A., Ferreira, F., and de Lusignan, S. (2018). Incidence and prevalence of cardiovascular disease in English primary care: a cross-sectional and follow-up study of the Royal College of General Practitioners (RCGP) Research and Surveillance Centre (RSC). BMJ Open *8*, e020282.
Hoerl, A.a.K., RW (1970). Ridge Regression: Biased Estimation for Nonorthogonal Problems. Technometrics *12*, 55-67.
Hoogeveen, R.M., Nahrendorf, M., Riksen, N.P., Netea, M.G., de Winther, M.P.J., Lutgens, E., Nordestgaard, B.G., Neidhart, M., Stroes, E.S.G., Catapano, A.L., et al. (2018). Monocyte and haematopoietic progenitor reprogramming as common mechanism underlying chronic inflammatory and cardiovascular diseases. Eur Heart J *39*, 3521-3527.
Huang, S.C., Everts, B., Ivanova, Y., O'Sullivan, D., Nascimento, M., Smith, A.M., Beatty, W., Love-Gregory, L., Lam, W.Y., O'Neill, C.M., et al. (2014). Cell-intrinsic lysosomal lipolysis is essential for alternative activation of macrophages. Nature immunology *15*, 846-855.
Humphries, K.H., Izadnegahdar, M., Sedlak, T., Saw, J., Johnston, N., Schenck-Gustafsson, K., Shah, R.U., Regitz-Zagrosek, V., Grewal, J., Vaccarino, V., et al. (2017). Sex differences in cardiovascular disease - Impact on care and outcomes. Front Neuroendocrinol *46*, 46-70.
Ifrim, D.C., Quintin, J., Joosten, L.A., Jacobs, C., Jansen, T., Jacobs, L., Gow, N.A., Williams, D.L., van der Meer, J.W., and Netea, M.G. (2014). Trained immunity or tolerance: opposing

907 functional programs induced in human monocytes after engagement of various pattern
908 recognition receptors. Clin Vaccine Immunol *21*, 534-545.
909 Jung, S.B., Choi, M.J., Ryu, D., Yi, H.S., Lee, S.E., Chang, J.Y., Chung, H.K., Kim, Y.K., Kang, S.G.,
910 Lee, J.H., et al. (2018). Reduced oxidative capacity in macrophages results in systemic insulin
911 resistance. Nat Commun *9*, 1551.
912 Kannan, Y., Perez-Lloret, J., Li, Y., Entwistle, L.J., Khoury, H., Papoutsopoulou, S., Mahmood, R.,
913 Mansour, N.R., Ching-Cheng Huang, S., Pearce, E.J., et al. (2016). TPL-2 Regulates Macrophage
914 Lipid Metabolism and M2 Differentiation to Control TH2-Mediated Immunopathology. PLoS
915 pathogens *12*, e1005783.
916 Kaufmann, E., Sanz, J., Dunn, J.L., Khan, N., Mendonca, L.E., Pacis, A., Tzelepis, F., Pernet, E.,
917 Dumaine, A., Grenier, J.C., et al. (2018). BCG Educates Hematopoietic Stem Cells to Generate
918 Protective Innate Immunity against Tuberculosis. Cell *172*, 176-190 e119.
919 Kim, S.H., and Reaven, G. (2013). Sex differences in insulin resistance and cardiovascular disease
920 risk. J Clin Endocrinol Metab *98*, E1716-1721.
921 Krenkel, O., Hundertmark, J., Abdallah, A.T., Kohlhepp, M., Puengel, T., Roth, T., Branco, D.P.P.,
922 Mossanen, J.C., Luedde, T., Trautwein, C., et al. (2020). Myeloid cells in liver and bone marrow
923 acquire a functionally distinct inflammatory phenotype during obesity-related steatohepatitis.
924 Gut *69*, 551-563.
925 Kurylowicz, A., Jonas, M., Lisik, W., Jonas, M., Wicik, Z.A., Wierzbicki, Z., Chmura, A., and
926 Puzianowska-Kuznicka, M. (2015). Obesity is associated with a decrease in expression but not
927 with the hypermethylation of thermogenesis-related genes in adipose tissues. J Transl Med *13*,
928 31.
929 Lam, R.S., O'Brien-Simpson, N.M., Holden, J.A., Lenzo, J.C., Fong, S.B., and Reynolds, E.C. (2016).
930 Unprimed, M1 and M2 Macrophages Differentially Interact with Porphyromonas gingivalis. PloS
931 one *11*, e0158629.
932 Langston, P.K., Shibata, M., and Horng, T. (2017). Metabolism Supports Macrophage Activation.
933 Front Immunol *8*, 61.
934 Leentjens, J., Bekkering, S., Joosten, L.A.B., Netea, M.G., Burgner, D.P., and Riksen, N.P. (2018).
935 Trained Innate Immunity as a Novel Mechanism Linking Infection and the Development of
936 Atherosclerosis. Circ Res *122*, 664-669.
937 Liang, C.P., Han, S., Senokuchi, T., and Tall, A.R. (2007). The macrophage at the crossroads of
938 insulin resistance and atherosclerosis. Circ Res *100*, 1546-1555.
939 Liao, Y., Smyth, G.K., and Shi, W. (2014). featureCounts: an efficient general purpose program
940 for assigning sequence reads to genomic features. Bioinformatics *30*, 923-930.
941 Liu, P.S., Wang, H., Li, X., Chao, T., Teav, T., Christen, S., Di Conza, G., Cheng, W.C., Chou, C.H.,
942 Vavakova, M., et al. (2017). alpha-ketoglutarate orchestrates macrophage activation through
943 metabolic and epigenetic reprogramming. Nat Immunol *18*, 985-994.
944 Luquain-Costaz, C., Lefai, E., Arnal-Levron, M., Markina, D., Sakai, S., Euthine, V., Makino, A.,
945 Guichardant, M., Yamashita, S., Kobayashi, T., et al. (2013). Bis(monoacylglycero)phosphate
946 accumulation in macrophages induces intracellular cholesterol redistribution, attenuates liver-X
947 receptor/ATP-Binding cassette transporter A1/ATP-binding cassette transporter G1 pathway,
948 and impairs cholesterol efflux. Arterioscler Thromb Vasc Biol *33*, 1803-1811.
949 Marks, J.B., and Raskin, P. (2000). Cardiovascular risk in diabetes: a brief review. J Diabetes
950 Complications *14*, 108-115.

951 Matyash, V., Liebisch, G., Kurzchalia, T.V., Shevchenko, A., and Schwudke, D. (2008). Lipid
952 extraction by methyl-tert-butyl ether for high-throughput lipidomics. J Lipid Res *49*, 1137-1146.
953 McCarthy, D.J., Chen, Y., and Smyth, G.K. (2012). Differential expression analysis of multifactor
954 RNA-Seq experiments with respect to biological variation. Nucleic Acids Res *40*, 4288-4297.
955 Mehlem, A., Hagberg, C.E., Muhl, L., Eriksson, U., and Falkevall, A. (2013). Imaging of neutral
956 lipids by oil red O for analyzing the metabolic status in health and disease. Nat Protoc *8*, 1149-
957 1154.
958 Moran, A., Jacobs, D.R., Jr., Steinberger, J., Steffen, L.M., Pankow, J.S., Hong, C.P., and Sinaiko,
959 A.R. (2008). Changes in insulin resistance and cardiovascular risk during adolescence:
960 establishment of differential risk in males and females. Circulation *117*, 2361-2368.
961 Nascimento, M., Huang, S.C., Smith, A., Everts, B., Lam, W., Bassity, E., Gautier, E.L., Randolph,
962 G.J., and Pearce, E.J. (2014). Ly6Chi monocyte recruitment is responsible for Th2 associated
963 host-protective macrophage accumulation in liver inflammation due to schistosomiasis. PLoS
964 pathogens *10*, e1004282.
965 Naylor, B.C., Porter, M.T., Wilson, E., Herring, A., Lofthouse, S., Hannemann, A., Piccolo, S.R.,
966 Rockwood, A.L., and Price, J.C. (2017). DeuteRater: a tool for quantifying peptide isotope
967 precision and kinetic proteomics. Bioinformatics *33*, 1514-1520.
968 Ng, M.K., Jessup, W., and Celermajer, D.S. (2001). Sex-related differences in the regulation of
969 macrophage cholesterol metabolism. Curr Opin Lipidol *12*, 505-510.
970 Nunemaker, C.S., Chung, H.G., Verrilli, G.M., Corbin, K.L., Upadhye, A., and Sharma, P.R. (2014).
971 Increased serum CXCL1 and CXCL5 are linked to obesity, hyperglycemia, and impaired islet
972 function. J Endocrinol *222*, 267-276.
973 Oh, D.Y., Morinaga, H., Talukdar, S., Bae, E.J., and Olefsky, J.M. (2012). Increased macrophage
974 migration into adipose tissue in obese mice. Diabetes *61*, 346-354.
975 Oiknine, J., and Aviram, M. (1992). Increased susceptibility to activation and increased uptake
976 of low density lipoprotein by cholesterol-loaded macrophages. Arterioscler Thromb *12*, 745-
977 753.
978 Opotowsky, A.R., McWilliams, J.M., and Cannon, C.P. (2007). Gender differences in aspirin use
979 among adults with coronary heart disease in the United States. J Gen Intern Med *22*, 55-61.
980 Paul, F., Arkin, Y., Giladi, A., Jaitin, D.A., Kenigsberg, E., Keren-Shaul, H., Winter, D., Lara-Astiaso,
981 D., Gury, M., Weiner, A., et al. (2016). Transcriptional Heterogeneity and Lineage Commitment
982 in Myeloid Progenitors. Cell *164*, 325.
983 Peters, S.A., Huxley, R.R., and Woodward, M. (2014). Diabetes as risk factor for incident
984 coronary heart disease in women compared with men: a systematic review and meta-analysis
985 of 64 cohorts including 858,507 individuals and 28,203 coronary events. Diabetologia *57*, 1542-
986 1551.
987 Pike Winer, L.S., and Wu, M. (2014). Rapid analysis of glycolytic and oxidative substrate flux of
988 cancer cells in a microplate. PLoS One *9*, e109916.
989 Potteaux, S., Gautier, E.L., Hutchison, S.B., van Rooijen, N., Rader, D.J., Thomas, M.J., Sorci-
990 Thomas, M.G., and Randolph, G.J. (2011). Suppressed monocyte recruitment drives
991 macrophage removal from atherosclerotic plaques of Apoe-/- mice during disease regression.
992 The Journal of clinical investigation *121*, 2025-2036.

993 Puleston, D.J., Buck, M.D., Klein Geltink, R.I., Kyle, R.L., Caputa, G., O'Sullivan, D., Cameron,
994 A.M., Castoldi, A., Musa, Y., Kabat, A.M., et al. (2019). Polyamines and eIF5A Hypusination
995 Modulate Mitochondrial Respiration and Macrophage Activation. Cell Metab *30*, 352-363 e358.
996 Qu, D., Liu, J., Lau, C.W., and Huang, Y. (2014). IL-6 in diabetes and cardiovascular
997 complications. British journal of pharmacology *171*, 3595-3603.
998 Robinson, M.D., McCarthy, D.J., and Smyth, G.K. (2010). edgeR: a Bioconductor package for
999 differential expression analysis of digital gene expression data. Bioinformatics *26*, 139-140.
1000 Roth, G.A., Johnson, C., Abajobir, A., Abd-Allah, F., Abera, S.F., Abyu, G., Ahmed, M., Aksut, B.,
1001 Alam, T., Alam, K., et al. (2017). Global, Regional, and National Burden of Cardiovascular
1002 Diseases for 10 Causes, 1990 to 2015. J Am Coll Cardiol *70*, 1-25.
1003 Rubinow, K.B. (2018). An intracrine view of sex steroids, immunity, and metabolic regulation.
1004 Mol Metab *15*, 92-103.
1005 Rudyk, M.P., Pozur, V.V., Voieikova, D.O., Hurmach, Y.V., Khranovska, N.M., Skachkova, O.V.,
1006 Svyatetska, V.M., Fedorchuk, O.G., Skivka, L.M., Berehova, T.V., et al. (2018). Sex-based
1007 differences in phagocyte metabolic profile in rats with monosodium glutamate-induced obesity.
1008 Sci Rep *8*, 5419.
1009 Rull, A., Camps, J., Alonso-Villaverde, C., and Joven, J. (2010). Insulin resistance, inflammation,
1010 and obesity: role of monocyte chemoattractant protein-1 (or CCL2) in the regulation of
1011 metabolism. Mediators Inflamm *2010*.
1012 Sanya, R.E., Webb, E.L., Zziwa, C., Kizindo, R., Sewankambo, M., Tumusiime, J., Nakazibwe, E.,
1013 Oduru, G., Niwagaba, E., Kabuubi Nakawungu, P., et al. (2019). The effect of helminth infections
1014 and their treatment on metabolic outcomes: results of a cluster-randomised trial. Clinical
1015 infectious diseases : an official publication of the Infectious Diseases Society of America.
1016 Shen, S.W., Lu, Y., Li, F., Shen, Z.H., Xu, M., Yao, W.F., Feng, Y.B., Yun, J.T., Wang, Y.P., Ling, W.,
1017 et al. (2015). The potential long-term effect of previous schistosome infection reduces the risk
1018 of metabolic syndrome among Chinese men. Parasite immunology *37*, 333-339.
1019 Shi, L., Pan, H., Liu, Z., Xie, J., and Han, W. (2017). Roles of PFKFB3 in cancer. Signal Transduct
1020 Target Ther *2*, 17044.
1021 Stanley, R.G., Jackson, C.L., Griffiths, K., and Doenhoff, M.J. (2009). Effects of Schistosoma
1022 mansoni worms and eggs on circulating cholesterol and liver lipids in mice. Atherosclerosis *207*,
1023 131-138.
1024 Stienstra, R., Netea-Maier, R.T., Riksen, N.P., Joosten, L.A.B., and Netea, M.G. (2017). Specific
1025 and Complex Reprogramming of Cellular Metabolism in Myeloid Cells during Innate Immune
1026 Responses. Cell Metab *26*, 142-156.
1027 Tacke, F., Alvarez, D., Kaplan, T.J., Jakubzick, C., Spanbroek, R., Llodra, J., Garin, A., Liu, J., Mack,
1028 M., van Rooijen, N., et al. (2007). Monocyte subsets differentially employ CCR2, CCR5, and
1029 CX3CR1 to accumulate within atherosclerotic plaques. The Journal of clinical investigation *117*,
1030 185-194.
1031 Tan, Y.Y., Gast, G.C., and van der Schouw, Y.T. (2010). Gender differences in risk factors for
1032 coronary heart disease. Maturitas *65*, 149-160.
1033 Taneja, V. (2018). Sex Hormones Determine Immune Response. Front Immunol *9*, 1931.
1034 Tibshirani, R. (1996). Regression shrinkage and selection via the lasso. J. R. Statist. Soc. B *58*,
1035 267–288.

1036 van der Windt, G.J., Everts, B., Chang, C.H., Curtis, J.D., Freitas, T.C., Amiel, E., Pearce, E.J., and
1037 Pearce, E.L. (2012). Mitochondrial respiratory capacity is a critical regulator of CD8+ T cell
1038 memory development. Immunity *36*, 68-78.
1039 Vats, D., Mukundan, L., Odegaard, J.I., Zhang, L., Smith, K.L., Morel, C.R., Wagner, R.A., Greaves,
1040 D.R., Murray, P.J., and Chawla, A. (2006). Oxidative metabolism and PGC-1beta attenuate
1041 macrophage-mediated inflammation. Cell Metab *4*, 13-24.
1042 Vernia, S., Cavanagh-Kyros, J., Barrett, T., Jung, D.Y., Kim, J.K., and Davis, R.J. (2013). Diet-
1043 induced obesity mediated by the JNK/DIO2 signal transduction pathway. Genes Dev *27*, 2345-
1044 2355.
1045 Willeit, J., Kiechl, S., Egger, G., Oberhollenzer, M., Oberhollenzer, F., Muggeo, M., Poewe, W.,
1046 and Bonora, E. (1997). The role of insulin in age-related sex differences of cardiovascular risk
1047 profile and morbidity. Atherosclerosis *130*, 183-189.
1048 Winn, N.C., Jurrissen, T.J., Grunewald, Z.I., Cunningham, R.P., Woodford, M.L., Kanaley, J.A.,
1049 Lubahn, D.B., Manrique-Acevedo, C., Rector, R.S., Vieira-Potter, V.J., et al. (2019). Estrogen
1050 receptor-alpha signaling maintains immunometabolic function in males and is obligatory for
1051 exercise-induced amelioration of nonalcoholic fatty liver. Am J Physiol Endocrinol Metab *316*,
1052 E156-E167.
1053 Wiria, A.E., Hamid, F., Wammes, L.J., Prasetyani, M.A., Dekkers, O.M., May, L., Kaisar, M.M.,
1054 Verweij, J.J., Guigas, B., Partono, F., et al. (2015). Infection with Soil-Transmitted Helminths Is
1055 Associated with Increased Insulin Sensitivity. PloS one *10*, e0127746.
1056 Wolde, M., Berhe, N., Medhin, G., Chala, F., van Die, I., and Tsegaye, A. (2019). Inverse
1057 Associations of Schistosoma mansoni Infection and Metabolic Syndromes in Humans: A Cross-
1058 Sectional Study in Northeast Ethiopia. Microbiol Insights *12*, 1178636119849934.
1059 Wolfs, I.M., Stoger, J.L., Goossens, P., Pottgens, C., Gijbels, M.J., Wijnands, E., van der Vorst,
1060 E.P., van Gorp, P., Beckers, L., Engel, D., et al. (2014). Reprogramming macrophages to an anti-
1061 inflammatory phenotype by helminth antigens reduces murine atherosclerosis. FASEB J *28*, 288-
1062 299.
1063 Wong, N.D., Zhao, Y., Patel, R., Patao, C., Malik, S., Bertoni, A.G., Correa, A., Folsom, A.R.,
1064 Kachroo, S., Mukherjee, J., et al. (2016). Cardiovascular Risk Factor Targets and Cardiovascular
1065 Disease Event Risk in Diabetes: A Pooling Project of the Atherosclerosis Risk in Communities
1066 Study, Multi-Ethnic Study of Atherosclerosis, and Jackson Heart Study. Diabetes Care *39*, 668-
1067 676.
1068 Zhou, Z., Subramanian, P., Sevilmis, G., Globke, B., Soehnlein, O., Karshovska, E., Megens, R.,
1069 Heyll, K., Chun, J., Saulnier-Blache, J.S., et al. (2011). Lipoprotein-derived lysophosphatidic acid
1070 promotes atherosclerosis by releasing CXCL1 from the endothelium. Cell Metab *13*, 592-600.
1071 Zou, H.a.H., T (2005). Regularization and variable selection via the elastic net. Journal of the
1072 Royal Statistical Society *67*, 301-320.
1073
1074
1075 **Figure legends**

1076 **Figure 1. Bone marrow derived macrophages (BMDM) from ApoE$^{-/-}$ male *S. mansoni***

1077 **infected mice exhibit increased oxygen consumption and mitochondria mass.** ApoE$^{-/-}$ male

1078 were fed HFD for 10 days before infection with *S. mansoni*. Ten weeks post infection mice were
1079 sacrificed and bone marrow cells were harvested and cultured for 7 days under M-CSF. (A)
1080 SeaHorse assay results for OCR of BMDC from infected and uninfected ApoE$^{-/-}$ males in basal
1081 conditions and in response to mitochondrial inhibitors. (B) Quantification (in picomoles per
1082 minute) of the basal oxygen consumption of BMDM from uninfected or infected ApoE$^{-/-}$ HFD
1083 male mice. (C) Quantification of the spare respiratory capacity of BMDM from uninfected or
1084 infected ApoE$^{-/-}$ HFD male mice (D) Extracellular acidification rate of BMDM from male
1085 uninfected or infected ApoE$^{-/-}$. (E) Oil Red O relative staining in BMDM from ApoE$^{-/-}$ mice (F)
1086 MitoTracker Red Deep Stain measure by flow cytometry in BMDM from ApoE$^{-/-}$ mice.
1087 SeaHorse assay analysis were performed the Seahorse XFe96 instrument. *$p < 0.05$; **$p < 0.01$;
1088 ***$p < 0.001$. Graphs are representative of multiple experiments (2-3), with n>4 per group.
1089

1090 Figure 2.
1091 **BMDM from male *S. mansoni* infected HFD ApoE$^{-/-}$ mice have increased TCA cycle usage**
1092 **and significantly reduced cholesterol esters.** A-E) Mϕ were differentiated from bone marrow
1093 of 10-week infected animals with M-CSF in a 7-day culture in normal glucose and then switched
1094 to ^{13}C-labeled glucose for 24 hours. F-H) Mϕs were differentiated with M-CSF in a 7-day culture
1095 and then total cellular lipids were extracted and analyzed via LC-MS based lipidomic analysis.
1096 F) PLS-DA derived score from HFD Infected and HFD Uninfected BMDM. G) Plot of lipid
1097 species from the BMDM of infected and uninfected males on HFD, significantly altered lipid
1098 species are red and labeled. H)Table of statistical analysis of VIP I) Box whisker plot of
1099 normalized AUC of cholesterol ester species, which were identified as VIP compounds from the
1100 PLS-DA analysis. J-L) Bone marrow macrophages were differentiated with M-CSF and mRNA
1101 sequenced via RNASeq. J) Volcano plot of significantly differentially expressed genes between

1102 BMDM from *S. mansoni* infected uninfected mice. K) iPathway analysis showed distinct profiles
1103 in BMDM from *S. mansoni* infected, mice. L,M) Total RNA was extracted from biologically
1104 independent BMDM differentiated in M-CSF for Real-time PCR validation of mgll and slc1a3
1105 regulation.
1106 Data in A-I are representative of 3 experiments with 4-6 mice per group in each experiment.
1107 Data in J and K are representative of sequencing of 2 biologically independent experiments with
1108 5-6 mice per group. Data in L are from 2 biologically independent experiments with 4-6 mice per
1109 group.
1110
1111 Figure 3
1112 ***S. mansoni* infection does not protect females from metabolic disease despite inducing**
1113 **alternative activation in hepatic macrophages**. (A-B) Total body weight and glucose tolerance
1114 test (GTT) at 10 weeks post-infection. GTT values were analyzed by Area Under the Curve and
1115 graphed using GraphPad Prims. (C) (D) Flow cytometry analysis of alternative activation
1116 markers CD206 and CD302 in perfused and digested livers gated on hepatic macrophages
1117 ($CD45^{+}CD64^{+}MertK^{+}$) Arg-1 expression in hepatic macrophages from uninfected and infected
1118 $ApoE^{-/-}$ mice Nos-2 expression by flow cytometry in hepatic macrophages 10 weeks post
1119 infection. (E) Ly6C expression in monocyte from peripheral blood mononuclear cells (PBMC) at
1120 10-week post infection by flow cytometry (F) MitoTracker Red in $CD115^{+}$ monocytes from
1121 PBMC at 10 weeks post immunization in uninfected and infected $ApoE^{-/-}$ mice. (G) Total cell
1122 counts from bone marrow cells utilizing trypan-blue discrimination of apoptotic cells (H)
1123 Percentages of CMP ($Lin^{-}CD127^{-}c\text{-}Kit^{+}Sca\text{-}1^{-}CD34^{+}CD16/32^{low}$) and GMP ($Lin^{-}CD127^{-}c\text{-}$
1124 $Kit^{+}Sca\text{-}1^{-}CD34^{+}CD16/32^{hi}$) (I) CMP cell counts in bone marrow $ApoE^{-/-}$ (J) GMP cell counts 10

1125 week post infection in ApoE$^{-/-}$ mice (K) Flow cytometry analysis of MDP defined as Lin^{-}c-
1126 Kit^{+}Sca-1^{-}FcγR^{low}CD34^{+}CD115^{+} (L) MDP cell counts in ApoE$^{-/-}$uninfected and infected male
1127 mice. Graphs are representative from experiments that were performed 3-4 times with n>4.
1128 Exception is MitoTracker data, which was performed twice, with n>4. Statistical analysis was
1129 done using unpaired Student's t test, *$p < 0.05$; **$p < 0.01$.
1130
1131 Figure 4.
1132 ***S. mansoni* infection induces sex-specific modulation of oxygen consumption and beta-**
1133 **oxidation in BMDM.** (A-C) oxygen consumption rate and spare respiratory capacity were
1134 measured at steady state. D-F) BMDM palmitate dependent oxygen consumption and spare
1135 respiratory capacity was measured in glucose limiting conditions. G) Oil Red O relative staining
1136 in BMDM from ApoE$^{-/-}$ mice (H) MitoTracker Red Deep Stain measure by flow cytometry in
1137 BMDM from ApoE$^{-/-}$ mice. SeaHorse assay analysis were performed the Seahorse XFe96
1138 instrument. *$p < 0.05$; **$p < 0.01$; ***$p < 0.001$. Graphs are representative of multiple
1139 experiments (2-3), with n>4 per group.
1140
1141 Figure 5.
1142 ***S. mansoni* infection induces significantly different cellular lipid profiles in BMDM from**
1143 **HFD female and male ApoE$^{-/-}$ mice.** A) PLS-DA derived score of LC-MS based lipidomic
1144 analysis of BMDM from HFD Infected females vs males. B) Box whisker plot of normalized
1145 AUC of cholesterol ester species, between female and male infected and uninfected HFD ApoE$^{-/-}$
1146 mice. C) PLS-DA derived score from Female HFD Infected and uninfected BMDM. D) Dot plot
1147 of lipid species identified in BMDM from infected and uninfected female ApoE$^{-/-}$ mice on HFD,

1148 significant lipid species are represented by red dots and labeled. E) Relative quantitation of BMP
1149 compounds in BMDM from male and female animals with and without *S. man*soni infection. F-I)
1150 Macrophages were differentiated with M-CSF in a 7-day culture with normal glucose and serum,
1151 and then switched to ^{13}C-labeled palmitate in dialyzed serum for 36 hours. J-N) Culture
1152 supernatants from BMDM stimulated with LPS for 24 hours were assayed for
1153 chemokines/cytokines. Data in A-E and J-N are representative of 2 biologically independent
1154 experiments with 4-8 mice per group. F-I are one experiment with 5-6 mice per group.
1155
1156

1157

1158 Figure 6.

1159 ***S. mansoni* infection differentially regulates the transcriptomes of BMDM from female and**
1160 **male ApoE$^{-/-}$ mice**. (A) Venn diagram showing upregulated genes in males only, independently
1161 of infection state and pathway analysis corresponding to the identified genes. (B) Venn diagram
1162 and pathway analysis of differentially expressed genes in males compared to females. (C) Gene
1163 ontology map of differentially expressed genes in response to *S. mansoni* infection in male
1164 compared to female ApoE $^{-/-}$ mice on HFD. Sequencing data are from one experiment with 5-6
1165 mice per group.

1166

1167 **Figure 7. *S. mansoni* induced modulation of male macrophage metabolism is long-lived in**
1168 **the absence of antigen.** Bone marrow from 10-week *S. mansoni* infected or control ApoE-/-
1169 mice on HFD was transferred into busulfan treated ApoE$^{-/-}$ recipients on HFD. A,B) Glucose
1170 tolerance test (GTT) at 10 weeks post-infection. GTT values were analyzed by Area Under the
1171 Curve and graphed using GraphPad Prism. C-E) Oxygen consumption rate and spare respiratory

1172 capacity were measured at steady state in 7day BMDM. F) MitoTracker Red Deep Stain measure

1173 by flow cytometry in BMDM. Data is two combined experiments 7-8 animals per group.

1174 Statistical analysis was done using Welch's t-tests.

1175

Figure 1

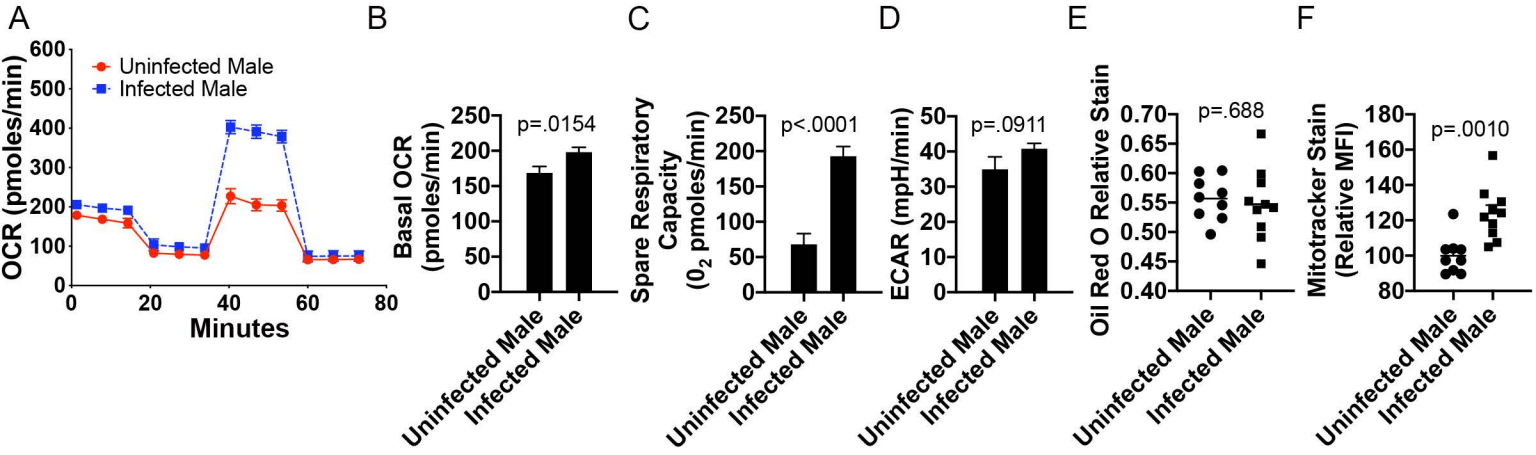
A
B
C
D
E
F
Uninfected Male
Infected Male
OCR (pmoles/min)
Minutes
Basal OCR (pmoles/min)
p=.0154
Spare Respiratory Capacity (0_2 pmoles/min)
p<.0001
ECAR (mpH/min)
p=.0911
Oil Red O Relative Stain
p=.688
Mitotracker Stain (Relative MFI)
p=.0010

Figure 2

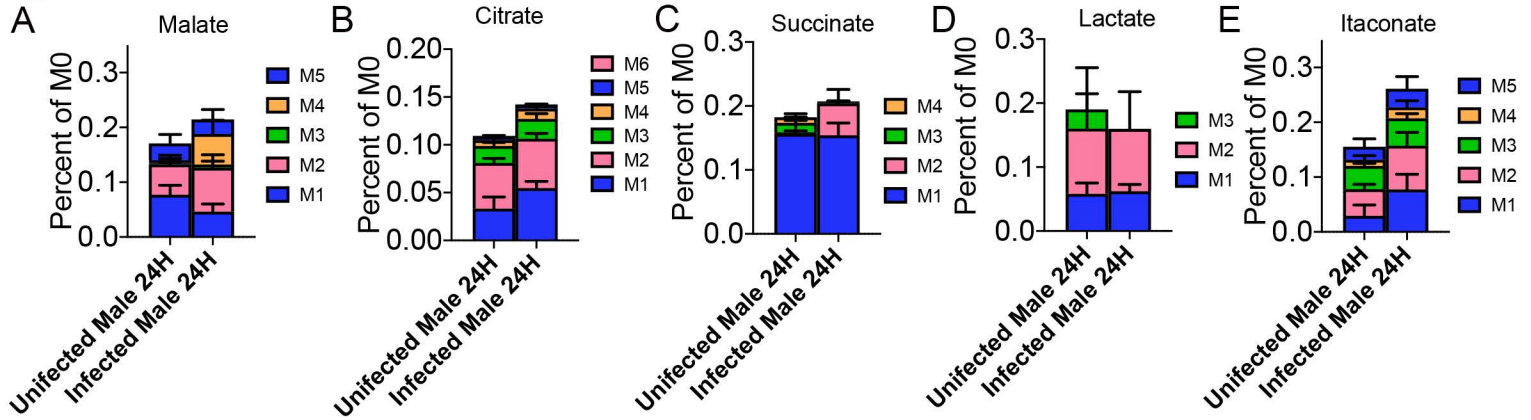

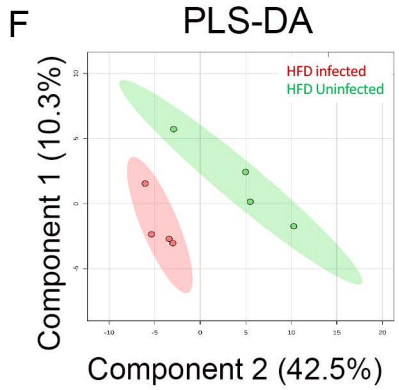

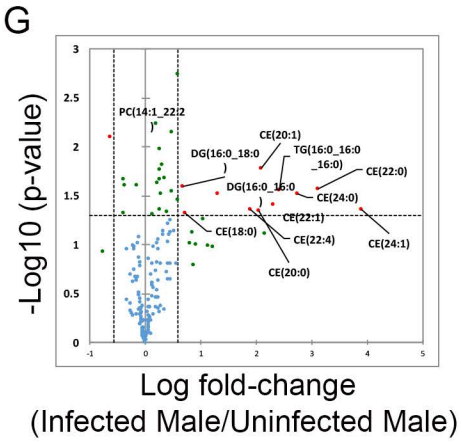

H

Name	Top ID	FC	log2(FC)	raw.pval	-log10(p)
CE_3048	CE(18:0)	0.61	-0.70209	0.047698	1.3215
CE_3259	CE(20:0)	0.24	-2.0498	0.045516	1.3418
CE_3025	CE(20:1)	0.24	-2.0828	0.01681	1.7744
CE_3388	CE(22:0)	0.12	-3.1123	0.027169	1.5659
CE_3239	CE(22:1)	0.20	-2.3098	0.039101	1.4078
CE_2793	CE(22:4)	0.27	-1.8932	0.044036	1.3562
CE_3458	CE(24:0)	0.15	-2.7462	0.030275	1.5189
CE_3378	CE(24:1)	0.07	-3.8946	0.043254	1.364
DG_2098	DG(16:0_16:0)	0.41	-1.2939	0.030364	1.5176
DG_2278	DG(16:0_18:0)	0.63	-0.67271	0.025481	1.5938
PC_1309	PC(14:1_22:2)	1.56	0.64476	0.0078633	2.1044
TG_2864	TG(16:0_16:0_16:0)	0.19	-2.4186	0.027936	1.5538

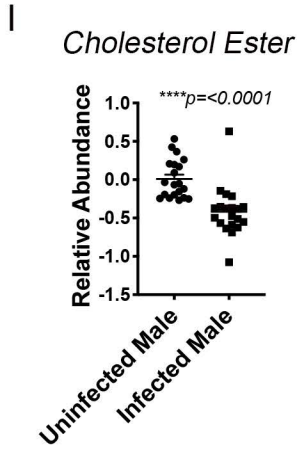

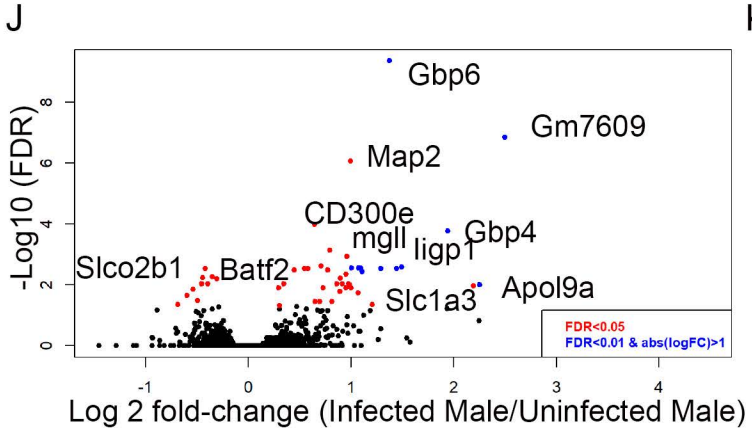

K

Pathway	P- value
Hematopoetic cell lineage	5.779E-08
Asthma	3.169E-05
Cytokine-Cytokine receptor interactions	0.0000894
Graft-versus host disease	0.0000894
Autoimmune thryroid disease	0.0000894
Type I Diabetes	0.0000894
Allograft rejection	0.0000894
Inflammatory bowel disease	0.0001406
Staphylococcus aureus infection	0.0001657
Cell adhesion molecules	0.0001722
Antigen processing and presentation	0.000212
Neuroactive ligand-receptor interaction	0.013
Phagosome	0.045

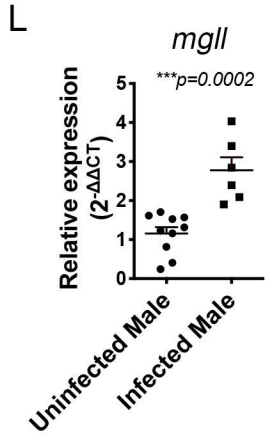

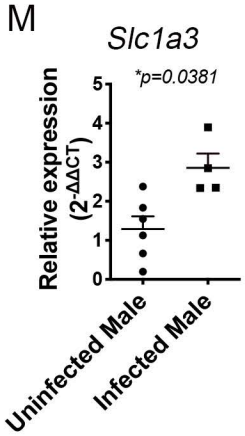

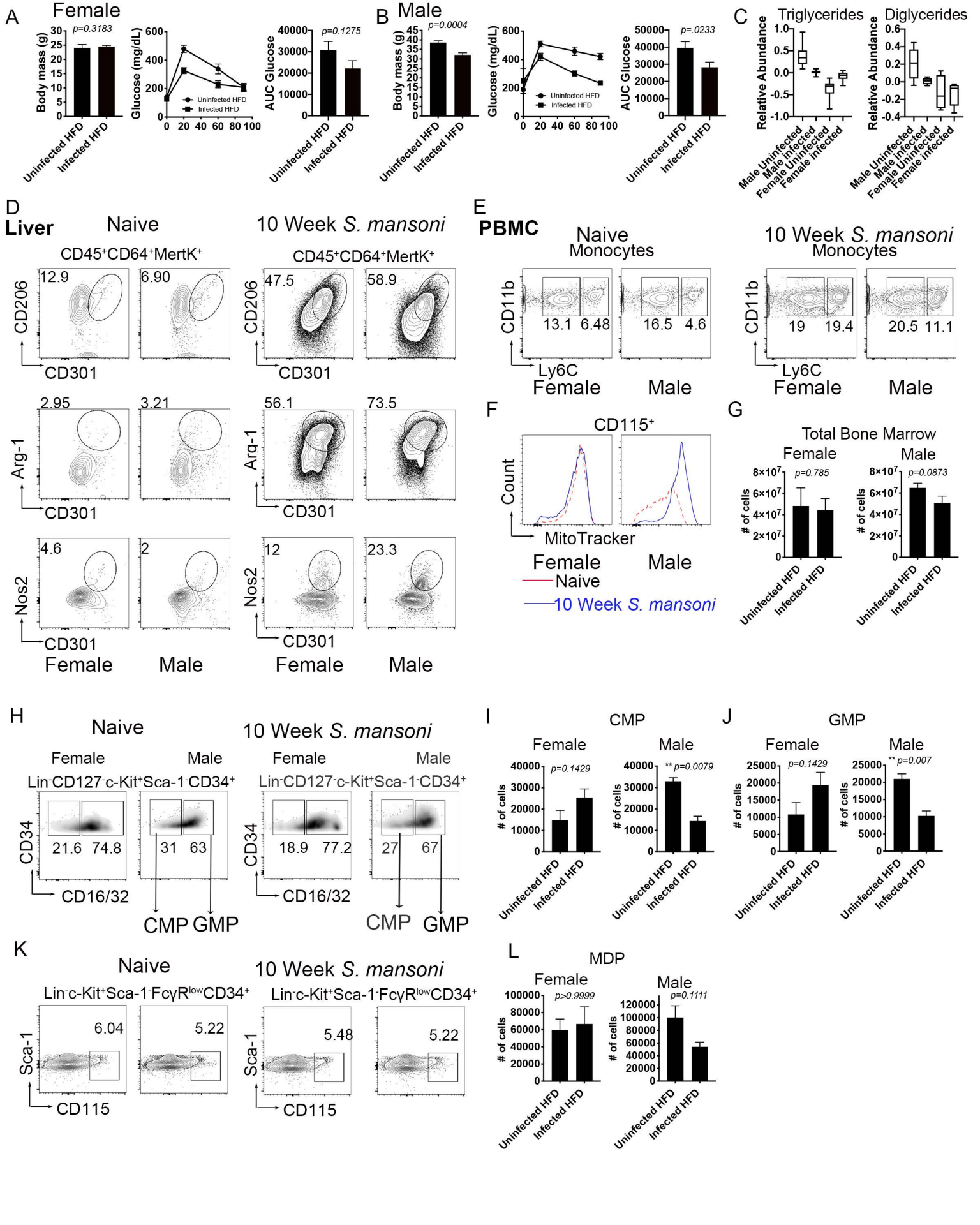
A
Female
p=0.3183
Body mass (g)
Uninfected HFD
Infected HFD
Glucose (mg/dL)
AUC Glucose
p=0.1275
B
Male
p=0.0004
p=.0233
C
Triglycerides
Diglycerides
Relative Abundance
Male Uninfected
Male Infected
Female Uninfected
Female Infected
D
Liver
Naive
10 Week S. mansoni
CD45+CD64+MertK+
CD206
CD301
Arg-1
Nos2
Female
Male
E
PBMC
Naive
Monocytes
10 Week S. mansoni
CD11b
Ly6C
F
CD115+
Count
MitoTracker
Naive
10 Week S. mansoni
G
Total Bone Marrow
# of cells
p=0.785
p=0.0873
H
Naive
10 Week S. mansoni
Lin-CD127-c-Kit+Sca-1-CD34+
CD34
CD16/32
CMP
GMP
I
CMP
p=0.1429
** p=0.0079
J
GMP
p=0.1429
** p=0.007
K
Lin-c-Kit+Sca-1-FcγRlowCD34+
Sca-1
CD115
L
MDP
p>0.9999
p=0.1111

Figure 4

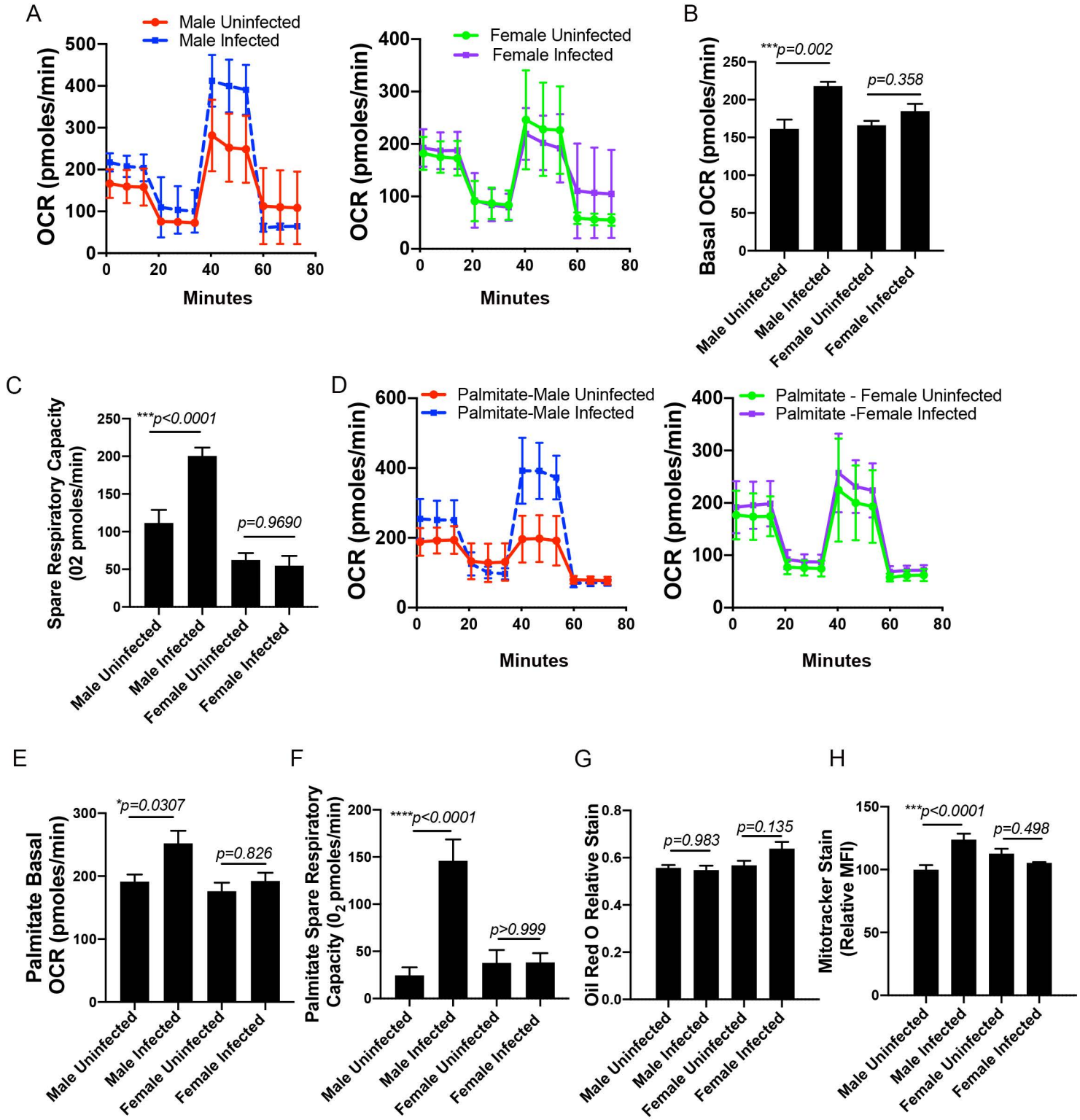
A
Male Uninfected
Male Infected
OCR (pmoles/min)
Minutes
Female Uninfected
Female Infected
B
***p=0.002
p=0.358
Basal OCR (pmoles/min)
Male Uninfected
Male Infected
Female Uninfected
Female Infected
C
***p<0.0001
p=0.9690
Spare Respiratory Capacity (02 pmoles/min)
D
Palmitate-Male Uninfected
Palmitate-Male Infected
Palmitate - Female Uninfected
Palmitate -Female Infected
E
*p=0.0307
p=0.826
Palmitate Basal OCR (pmoles/min)
F
****p<0.0001
p>0.999
Palmitate Spare Respiratory Capacity (0_2 pmoles/min)
G
p=0.983
p=0.135
Oil Red O Relative Stain
H
***p<0.0001
p=0.498
Mitotracker Stain (Relative MFI)

Figure 5

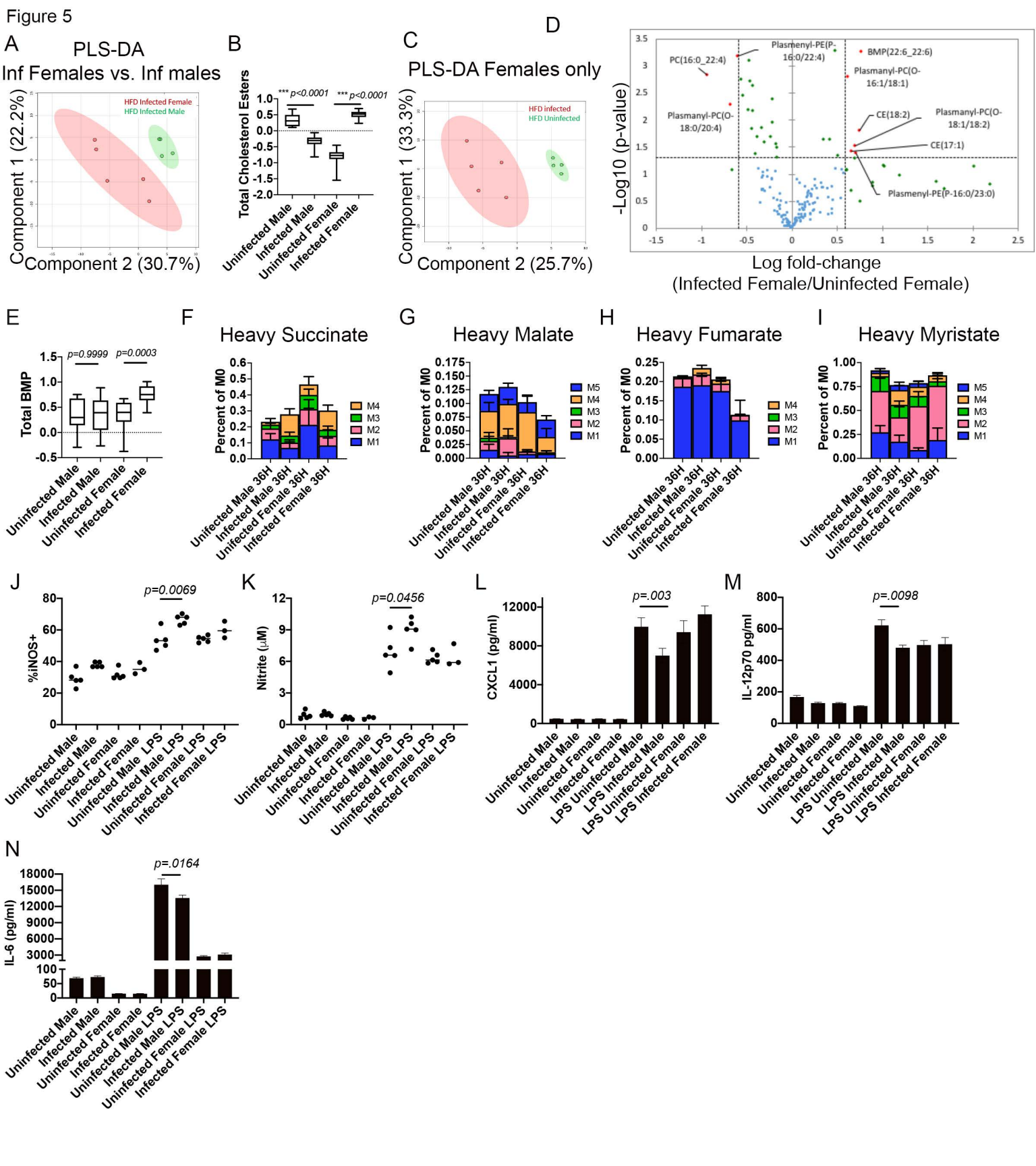
A
PLS-DA
Inf Females vs. Inf males
HFD Infected Female
HFD Infected Male
Component 1 (22.2%)
Component 2 (30.7%)
B
Total Cholesterol Esters
*** p<0.0001
*** p<0.0001
Uninfected Male
Infected Male
Uninfected Female
Infected Female
C
PLS-DA Females only
HFD infected
HFD Uninfected
Component 1 (33.3%)
Component 2 (25.7%)
D
-Log10 (p-value)
Log fold-change
(Infected Female/Uninfected Female)
PC(16:0_22:4)
Plasmenyl-PE(P-16:0/22:4)
BMP(22:6_22:6)
Plasmanyl-PC(O-16:1/18:1)
Plasmanyl-PC(O-18:0/20:4)
CE(18:2)
Plasmanyl-PC(O-18:1/18:2)
CE(17:1)
Plasmenyl-PE(P-16:0/23:0)
E
Total BMP
p=0.9999
p=0.0003
F
Heavy Succinate
Percent of M0
G
Heavy Malate
H
Heavy Fumarate
I
Heavy Myristate
M5
M4
M3
M2
M1
Uninfected Male 36H
Infected Male 36H
Uninfected Female 36H
Infected Female 36H
J
%iNOS+
p=0.0069
K
Nitrite (μM)
p=0.0456
L
CXCL1 (pg/ml)
p=.003
M
IL-12p70 pg/ml
p=.0098
N
IL-6 (pg/ml)
p=.0164
Uninfected Male
Infected Male
Uninfected Female
Infected Female
Uninfected Male LPS
Infected Male LPS
Uninfected Female LPS
Infected Female LPS

Figure 6

A Upregulated genes in males

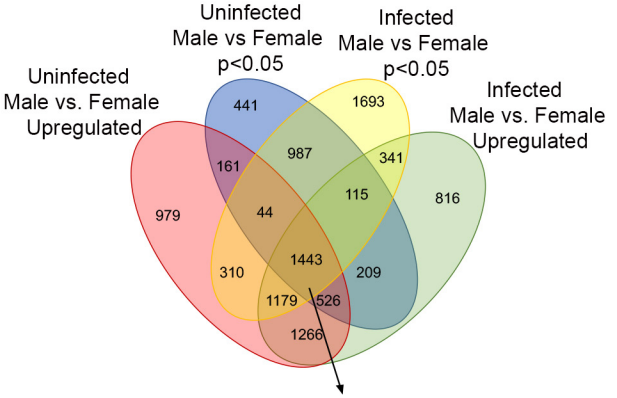

Pathways	Number of genes
Metabolism	238
Innate Immune System	216
Gene expression	183
Metabolism of proteins	149
Class I MHC Mediated Antigen Processing	85
Cell cycle	76
Vesicle mediated transport	72
Unassigned	63
Regulation of TP53 activity	52
NK-KappaB Signaling	47
DNA Double-strand break repair	42
Organelle biogenesis and maintenance	42
TNFR1 Pathway	31

B Differential regulation in male vs. female

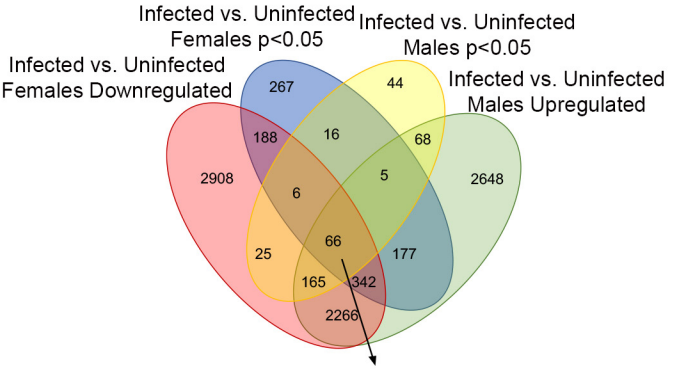

Pathways	Number of genes
Unassigned	31
Metabolism	10
Hemostasis	6
Adaptive immune system	2
Collagen degradation	2
Developmental biology	2
Metabolism of proteins	2
Neurotransmitter receptors and postsynaptic signal transmission	2
ROS and RNS production in phagocytes	2
Signal transduction	2

C Gene Ontology Map

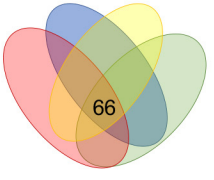

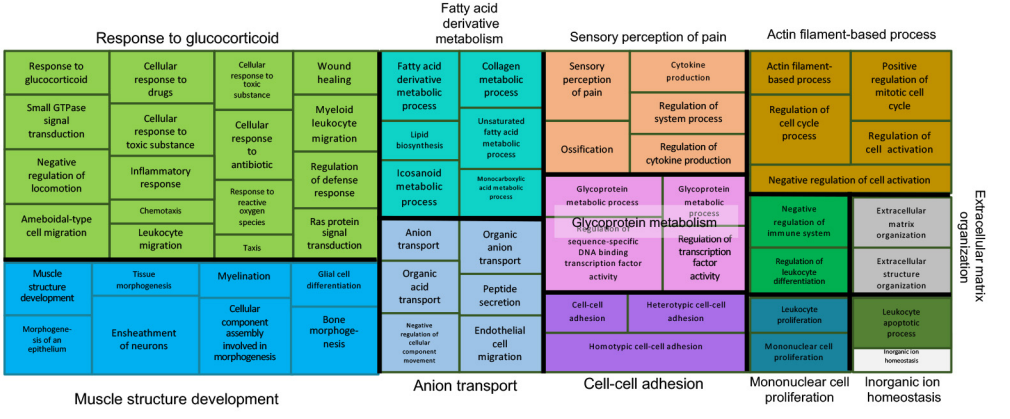

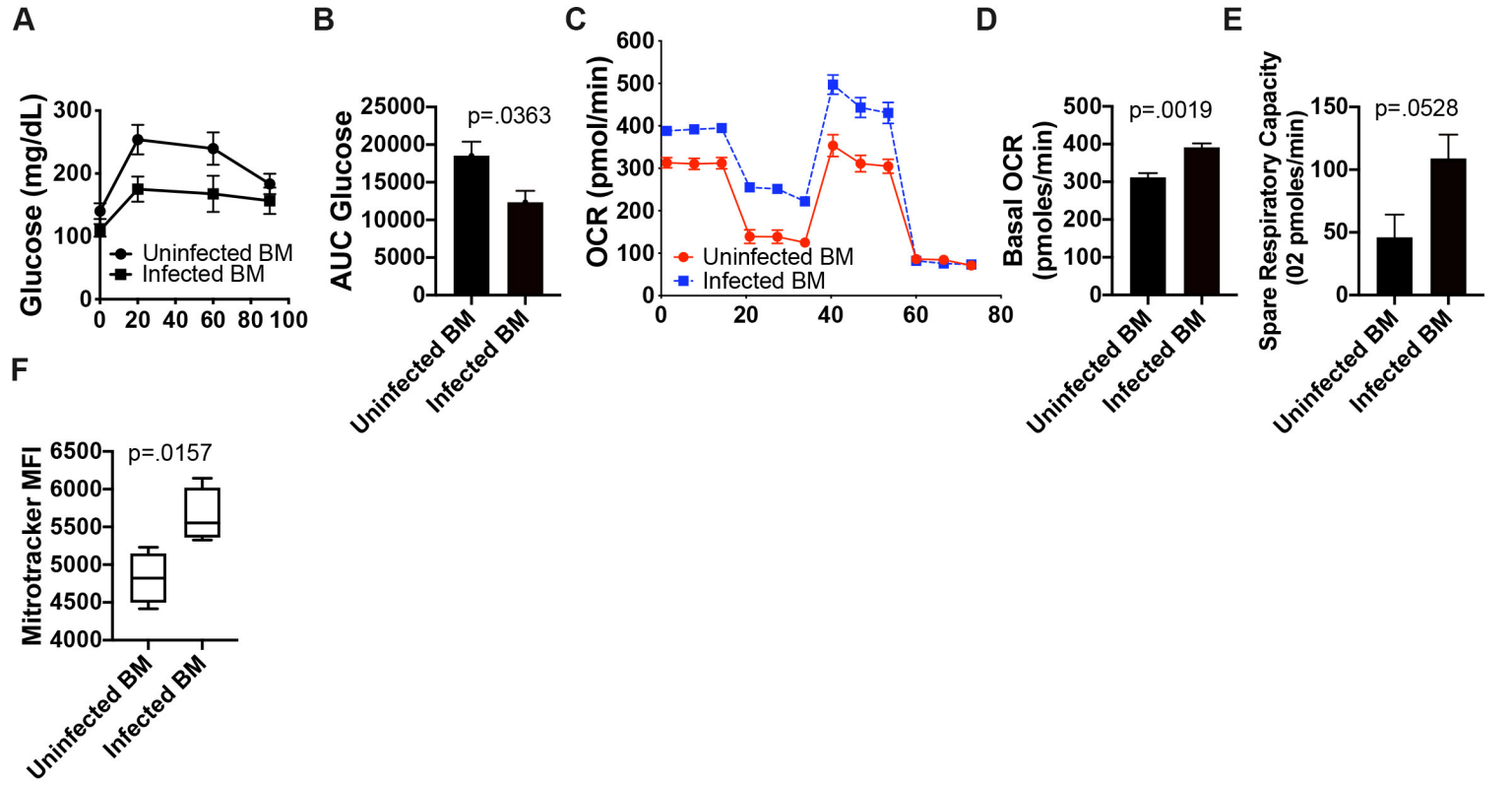
A
Glucose (mg/dL)
300
200
100
0
0 20 40 60 80 100
Uninfected BM
Infected BM
B
AUC Glucose
25000
20000
15000
10000
5000
0
p=.0363
Uninfected BM
Infected BM
C
OCR (pmol/min)
600
500
400
300
200
100
0
0 20 40 60 80
Uninfected BM
Infected BM
D
Basal OCR (pmoles/min)
500
400
300
200
100
0
p=.0019
Uninfected BM
Infected BM
E
Spare Respiratory Capacity (02 pmoles/min)
150
100
50
0
p=.0528
Uninfected BM
Infected BM
F
Mitrotracker MFI
6500
6000
5500
5000
4500
4000
p=.0157
Uninfected BM
Infected BM